Summer 8-19-2022

# Contact Dewatering of Cellulose Nanofibers for Biopolymer Composite Applications

Alexander Collins
*University of Maine*, alexander.w.collins@maine.edu

# CONTACT DEWATERING OF CELLULOSE NANOFIBERS FOR BIOPOLYMER COMPOSITE APPLICATIONS

By

Alexander Collins

B.S. Bioengineering, University of Maine, 2015

M.S. Forest Resources, University of Maine, 2022

A THESIS

Submitted in Partial Fulfillment of the

Requirements for the Degree of

Master of Science

(in Forest Resources)

The Graduate School

The University of Maine

August 2022

Advisory Committee:

Mehdi Tajvidi, Associate Professor of Renewable Nanomaterials, Advisor

Dr. Douglas Gardner, Professor of Sustainable Materials and Technology, University of Maine

Dr. William Gramlich, Associate Professor of Chemistry, University of Maine

# CONTACT DEWATERING OF CELLULOSE NANOFIBERS FOR BIOPOLYMER COMPOSITE APPLICATIONS

Alexander Collins

Thesis Advisor: Dr. Mehdi Tajvidi

An Abstract of the Thesis Presented
in Partial Fulfillment of the Requirements for the
Degree of Master of Science
(in Forest Resources)
August 2022

Cellulose Nanofibrils (CNFs) are promising materials for reinforcement of polymer matrices attributable to their impressive physical and mechanical properties, as well as their biodegradability. However, the utilization of these materials in composites is made challenging by the water content of CNF slurries, the tendency of CNFs to agglomerate as they dry, and incompatibility between hydrophilic CNFs and hydrophobic polymer matrices. The most commercially viable drying methods to produce small-scale dry CNFs, such as spray drying, are very energy intensive, can only dry the materials down to micron-scale agglomerates, and do not preserve fibrillar aspect ratios. “Contact dewatering,” or the removal of bound water from CNF suspensions using wood flour (WF) and mechanical pressing, may provide a solution to the challenge of excess water and preservation of nanoscale CNF dimensions after drying. This project explored the use of contact dewatering with maple wood flour to remove water from CNF suspensions and incorporate dry CNF into poly(lactic) acid (PLA) composites as part of hybrid WF-CNF furnishes. This concept was further explored by using cryocrushed PLA powder instead of wood flour to dewater and process CNF into PLA-CNF composites. The use of WF showed preservation of nanoscale CNFs on the surface of wood particles after drying and high energy efficiency in water removal from CNF suspensions, with mixed results in terms of mechanical properties when incorporated into wood-plastic composites. These results included a slight increase in tensile modulus compared to PLA with WF at the lowest wt.%CNF/LCNF hybrid furnish, a drop in tensile strength with higher wt.%CNF/LCNF loading levels, and a reduction in flexural strength at lower wt.%CNF/LCNF loading

levels. When successfully scaled-up to produce 50lbs of a PLA/WF/CNF composite for additive manufacturing, the process showed an 84% decrease in specific drying energy per gram of dried CNF compared to empirical values for spray-dried CNF (SDCNF). The use of small polymer particles as opposed to wood in the contact dewatering process for drying and direct compounding of CNF into composites has not been extensively studied, so the viability of contact dewatering with poly(lactic) acid (PLA) powder as a dewatering method for compounded PLA/CNF composites in terms of energy efficiency, preservation of nanoscale CNF morphology, and mechanical properties was also evaluated. Initial results that utilized high or equivalent amounts of CNF to PLA in the dewatering process showed some preservation of nanoscale morphology of dry CNFs, but with overall structures that favored spherical agglomerates with low aspect ratios that reduced the mechanical properties of the final composites compared to PLA and PLA/SDCNF. Using lower amounts of CNF in the dewatering process reduced the formation of larger-scale agglomerates, which was optimized to produce micron-to-nano-scale fibrillar CNF structures observed under polarized light microscopy (PLM). Attempting to model CNF agglomeration around PLA particles by assuming the formation of spherical agglomerates based on CNF weight percent and PLA particle size was not accurate to observed results for agglomeration based on the weight percent of CNF. Using PLA for contact dewatering showed more efficient water removal from the CNF suspension than previous wood flour-CNF furnishes, and specimens laser cut from compression molded films of dried materials showed an increase in tensile strength of up to 31% compared to pure PLA. Shear-mixed specimens showed an increase in tensile strength and modulus of 1.7% and 4.2% compared to PLA at 1 and 2wt.%CNF loading levels, respectively, and had equivalent or better properties than PLA-Spray Dried CNF at the same loading levels. None of these results were statistically significant save for significantly higher tensile modulus in dewatered CNF composites compared to SDCNF composites at 1 and 2wt.% total CNF loading levels post-shear-mixing. Theoretical energy for drying dewatered CNF to produce micron-to-nanoscale dry fibrils after one press was 67-205x lower than empirical values for drying SDCNF depending on initial CNF loading level.

## DEDICATION

To Dr. Sonja Birthisel and the Wilson Center for providing me a space for spiritual and personal exploration during my studies.

To my lab mates: Ikram, Musfiqr, Rakibul, Tauhid, Islam, Wenjing, Cong, and Nabanita for making the LRN a pleasant working community!

To my landlord David J. Erker, who provided me with shelter and fatherly guidance during some of the most difficult times.

To my family, who show time and time again they will come through for me when the chips are down.

To my dear friends and comrades, Silas and Dan. Whenever I lose faith in myself, you are always there to help me find it again. Until the ends of the Earth.

To my advisor, Dr. Mehdi Tajvidi. His patience and wisdom guided me through my Master's journey.

## ACKNOWLEDGEMENTS

This work was supported in part by funding from UT-Batelle LLC (Oak Ridge National Laboratories) with the United States Department of Energy under contract DE-AC05-00OR2275 (subcontract # 4000174848)

Emma Perry from the UMaine Electron Microscopy Laboratory for assistance with SEM

Chris West, Lu Wang, and Justin Crouse from the UMaine Advanced Structures and Composites Center for their assistance with composite compounding, molding, and testing

Russell Edgar and Timothy Degnan from the UMaine Advanced Structures and Composites Center for their assistance with dewatering scale-up operations

Mehdi Tajvidi, William Gramlich, and Douglas Gardner for being on this thesis committee

**TABLE OF CONTENTS**

## LIST OF TABLES

## LIST OF FIGURES

## LIST OF EQUATIONS

## LIST OF ABBREVIATIONS

CNF/CNFs: Cellulose Nanofiber/Nanofibers

LCNF/LCNFs: Lignin-Containing Cellulose Nanofiber/Nanofibers

SDCNF/SDCNFs: Spray-Dried Cellulose Nanofiber/Nanofibers

dCNF/dCNFs: Dewatered Cellulose Nanofiber/Nanofibers

PLA: Poly(lactic) Acid

WF: Wood Flour

# CHAPTER 1

# INTRODUCTION

## 1.1. CNF, PLA, and Challenges

Because of the adverse effects of petroleum-based polymers on human health and the environment[1][2], as well as the dwindling supply of oil reserves required to produce these polymers[3], there is a societal need for bio-based, sustainable replacements. Along with commercial thermoplastic biopolymers such as poly(lactic) acid (PLA)[4], much research has been conducted in the use of cellulose, the most abundant naturally occurring polymer on Earth[5]. In particular, cellulose nanofibrils (CNFs), the fundamental structural elements of plants, have shown promise attributed to their high theoretical mechanical properties[6][7], inherent biodegradability due to susceptibility to hydrolysis and enzymatic degradation[8], low environmental or human health and safety risks[9], and potential to be manufactured with minimum modification of existing paper pulping infrastructure and equipment. The production of these materials from bleached kraft pulp produced via pulp-making machinery could provide a potential economic avenue for the nation's flagging paper industry[10], and provide similar opportunities to rural, heavily forested areas around the world. If used as a reinforcement material for polymers from renewable resources, such as PLA, CNFs have promise as a material for making fully compostable natural fiber-plastic composites for consumer, construction, aerospace, and automotive applications.

The potential of CNFs for use in natural fiber-plastic composites, however, is hampered by the tendency of CNFs to irreversibly "agglomerate" (stick together and form larger clumps or sheets) during drying attributable to strong fiber-fiber hydrogen bonding and the high surface tension of water pulling fibers together during evaporation[11]. This agglomeration reduces length/width (aspect) ratios of the fibers, reducing their reinforcement capability for plastic composites[12]. CNFs made from paper pulp are often produced in slurries at low weight percent solids in water, the presence of which in the system further complicates compounding with more hydrophobic polymer resins. This water content also causes issues with transportation, as a metric ton of wet CNFs (1000 kg) can contain as little as 30kg of CNFs by

dry weight, and transportation can cost as much as $115/ton of material per 500 miles[13]. Research has been conducted into multiple methods for drying, such as conventional oven drying, freeze drying, supercritical and spray drying, but few methods have effectively preserved the nanoscale structure of CNFs or its high aspect ratios after drying[11]. CNFs also present challenges as an engineering material due their labor - and energy-intensive production process, making energy optimization critical for their use as a "sustainably sourced" material[9]. Spray drying, which is seen as the process that most reliably produces small-scale dried material from CNFs, has a high energy cost[14], making the search for a less energy-intensive drying method more important.

### 1.2. Contact Dewatering

Previous research has shown that water can be removed from suspensions of CNFs by mixing them with wood flour, and then pressing them in a typical cold press used for wood composite manufacture[15]. In this process, known as "contact dewatering[16]," bound water in the CNF suspension is converted into free water attributable to favorable surface interactions between CNFs and wood fibers, allowing it to be removed out of the system via methods such as mechanical pressing. This reduces the amount of water that needs to be dried via conventional methods. The dewatering process can also be used with lignin-containing CNFs (LCNFs)[17] from unbleached wood pulp or recycled old corrugated cardboard (OCC) pulp. The lignin content increases the hydrophobicity of the CNFs, which can act as a compatibilizer and potentially improve the compatibility of CNFs with nonpolar polymers[18][19]. Some experiments utilizing CNFs bound to wood flour have also shown the retention of some nanoscale structure of CNFs attached to wood flour after freeze drying[20], as well as a slight increase in tensile and flexural properties of a polypropylene (PP) matrix when compounded with a maleic anhydride-PP compatibilizer. Another method that pre-mixed high density polyethylene (HDPE) pellets with wood flour, CNFs, and a maleic anhydride-PE compatibilizer before freeze-drying saw a 93, 154, and 117% increase in flexural strength, flexural modulus, and impact strength, respectively, in the final small-scale HDPE/wood flour/CNF composite[21]. To our knowledge, no method has found significant improvements in mechanical properties

utilizing mixtures of CNFs and wood flour without the use of a freeze-drying process. In addition, no method has fully explored the energy use of the dewatering process for a mixture of wood flour and CNFs for use in composites.

### 1.3. Thesis Objectives and Approach

This work examines the efficacy and efficiency of contact dewatering for producing dry CNF fibrils for use in biopolymer composite applications. The first part of this research focused on the use of wood flour (WF) to dewater and dry CNFs and LCNFs similar to previous methods for the manufacture of hybrid PLA/WF/CNF composites, with a focus on preserving nanoscale morphology after drying, mechanical properties of final composites, and drying energy. The second part of this research examined CNF dewatering with micron-scale particles of PLA to produce pre-mixed dewatered/dried PLA-CNF for composite processing, with a similar focus on morphology, mechanical properties, and drying energy. The overall objectives are to demonstrate facile processing methods for CNFs for use in biopolymer composites that can produce similar or better properties to spray dried CNFs (SDCNFs) without complex or energy-intensive drying processes.

# CHAPTER 2

# CONTACT DEWATERING CNF WITH WF FOR HYBRID COMPOSITES

## 2.1. Chapter Summary

In this work, the viability of contact dewatering of cellulose nanofibrils (CNFs) and lignin-containing cellulose nanofibrils (LCNFs) was tested to achieve nanoscale morphology of dried fibers on wood particles with varying CNF and LCNF contents after dewatering and oven drying. Nanoscale dimensions of dried CNFs and LCNFs were observed on the surface of wood particles, and mechanical testing of WF-CNF and WF-LCNF furnish-incorporated poly(lactic) acid (PLA) composites showed similar or better properties than PLA mixed with spray-dried CNFs. Analysis of theoretical energy required to dry CNFs and LCNFs via contact dewatering showed a great reduction compared to non-dewatered CNFs. Scaling up the dewatering process to produce 50 lbs of composite material for large scale additive manufacturing while measuring energy inputs also showed a 6-fold decrease in specific drying energy for dewatered CNFs compared to spray dried CNFs.

## 2.2. Introduction

This work utilized the method of contact dewatering CNFs and LCNFs with wood flour for use in wood-plastic composites. CNFs/LCNFs were combined with wood flour (WF) at different WF/CNF and WF/LCNF ratios, dewatered, dried, and characterized to assess macroscale and nanoscale structure. Wood flour-CNF (WF-CNF) furnishes were then melt-compounded with PLA to produce wood-plastic composites, which were tested for flexural, tensile, and impact strengths. The properties of these composites were compared to pure PLA (no reinforcement), PLA with dewatered wood flour (no CNFs), and PLA with spray dried CNFs. WF-CNFs and WF-LCNFs were also pressed multiple times to determine the efficiency of water removal via the dewatering method, and the energy costs of drying dewatered WF-CNF and WF-LCNF via oven drying were compared to drying conventional slurries of CNFs to determine if contact dewatering provides a more energy efficient alternative to producing dried

CNFs. The aim was to produce large-scale, fully bio-based composites with CNF using facile drying methods for 3D printing applications.

## 2.3. Materials and Methods

### 2.3.1. Furnish Manufacture and Characterization

Cellulose Nanofibrils (90% fines, ~3 wt.% solids)) made from bleached softwood kraft pulp were sourced from the UMaine Process Development Center. Lignin-Containing Cellulose Nanofibrils were produced using a Masuko Super Mass Colloider (Kawaguchi, Japan) by further refining of a stock of LCNF produced from recycled old corrugated container (OCC) fibers (70% fines, ~20 wt.% solids) to 90% fines and 2 wt.% solids at the UMaine Process Development Center. Maple wood flour (60-80mesh or 177-250μm) was sourced from Lignetics (Louisville, Colorado).

The overall furnish preparation process is summarized in Figure 1. CNFs or LCNFs were mixed with wood flour at different percent CNF/LCNF contents (0, 10, 30, 50 wt.%), targeting 5% total solids per mixture. The LNCFs were vacuum filtered to ~3.5% solids, then diluted to ~3% solids to match the starting solids content of the CNFs. First, the calculated amount of water was added to the CNFs or LCNFs , then wood flour was added and mixed with the suspension. The entire wet furnish was blended by a KitchenAid Artisan 5 stand mixer (St. Joseph, Michigan) at power setting 1 for 3 min. Approximately 1g of each freshly mixed sample was analyzed with a moisture content analyzer to determine starting percent solids content, and 100-150 g of each mixture at a time was dewatered via cold pressing with a DAKE (Grand Haven, MI) hydraulic press. A square mold was used to contain the material, which was pressed at ~2.2 MPa (63.5 $in^2$ press area). Mesh screens were placed underneath the pressing area and on top of the furnish in the mold in to evenly distribute pressure and ensure water removal, and paper towels were placed underneath the bottom mesh to prevent pooling and re-absorption of removed water by the furnish.

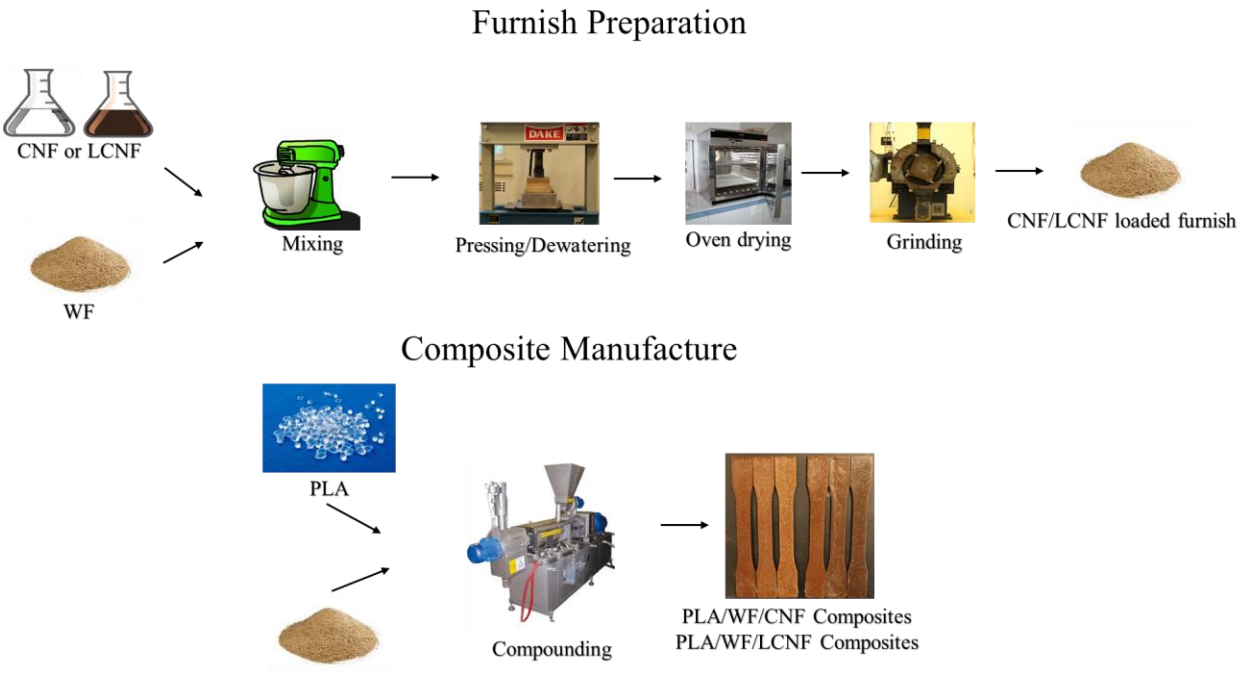


Figure 1: Outline for overall experiment design for this work: furnish dewatering, drying, and grinding process, followed by composite manufacture process.

The dewatered furnishes were broken up into smaller wet pellets by the KitchenAid mixer (power setting 2, 3 min), then dried in a Fisherbrand Isotherm oven (Fischer Scientific, Waltham, MA) at 120 ℃ for 6 hours. Dried samples were then homogenized in a Wiley Mill (Thomas Scientific, Swedesboro, New Jersey) utilizing a mesh sieve screen with 1 mm openings. Pictures of the homogenized WF-CNF and WF-LCNF furnishes were taken for particle size analysis, using a ruler for scale in the images. ImageJ software[22] was used to analyze the distributions of fiber lengths and aspect ratios for each furnish type. To determine the difference in diameter between maple WF and dry WF-CNF mixtures, sieve analysis was performed (Retsch, Newtown, PA) using sieve pans (Gilson Company, Lewis Center, OH) with 500, 425, 250, 180, and 150 μm mesh sizes (US mesh size: 35, 40, 60, 80, and 100, respectively). Sieve pans were weighed, then 10 g of each furnish was sieved with an amplitude of 1 for 20 minutes, after which pans were weighed again, and fiber mass for each sieve size was determined be subtracting the empty pan mass from the sieved pan mass. The mass percent of each fractions size was determined by dividing the

fiber mass for each sieve size by the total collected fiber mass of the furnish. Samples of all homogenized furnishes were also visualized at the nanoscale with scanning electron microscopy (SEM) to observe nanoscale structure of dewatered CNF bound to wood flour. For SEM, samples were dispersed on top of carbon-tape coated SEM stages, after which they were sputter coated with 4 nm of a gold/palladium material to provide a conductive layer over the samples. The SEM used was a Zeiss Nvision 40 (Oberkochen, Germany) at 3kV.

### 2.3.2. Composite Processing and Testing

Spray-Dried CNFs (SDCNFs, 90% fines) were sourced from the UMaine Forest Bioproducts Research Institute using a large-scale custom spray drier (GEA NIRO, Columbia, MD). SDCNFs were produced from a 3 wt.% CNF slurry diluted down to 1 wt.% solids, which was then dried at 125°C with a 30,000 rpm atomizer. PLA pellets (Natureworks Ingeo 4043D, Minnetonka, MN) were ground in a granulating mill (Hellweg Maschinenbau, Roetgen, Germany)(U.S. screen size #12) for easier compounding with the WF-CNF/LCNF furnishes from the previous section, and all materials including SDCNFs were dried for 4-16 hours (55-60 ℃ for PLA and 100-103 ℃ for furnishes/CNFs, respectively) before compounding via a Brabender co-rotating twin screw extruder (Brabender, South Hackensack, NJ) at 230 ℃ with a screw speed of 60 rpm. Composites were manufactured to 20 wt.% total loading of furnish, and corresponding PLA/WF/CNF and PLA/WF/LCNF compositions are displayed in Table 1. Controls were made with 20 wt.% maple wood flour, dewatered, dried, and ground in the same method as other furnishes, pure PLA, and PLA with 20 wt.% spray dried CNF. Extruded composites were pelletized in the same granulating mill used to pelletize PLA (U.S. screen size #6), and stored at ~55 ℃ overnight to remove moisture before injection molding. Pellets were injection molded (Electro-Matic Inc, Farmington Hills, MI) at 190 ℃ into specimens for ASTM D-790[23] (flexure) and D-7205[24] (tensile) standard specimens. Specimens were conditioned at ~25 °C and ~50% relative humidity for at least 48 hours prior to testing. At least N = 5 specimens per sample type were tested with 3 point-bending (500N load cell, crosshead speed = 1.82 mm/min) and tensile (100kN load cell, test rate = 5 mm/min) apparatus in an Instron model #5942 and Instron model #5966 universal test machine (Instron, Norwood, MA),

respectively. Since the PLA composites were much more likely to have brittle failure mechanisms without a definitive "yield" point, tensile strengths were reported in terms of tensile strain at break, not yield. Intact portions of broken specimens from flexural testing were cut to size and notched according to ASTM D-256[25] for impact testing, conditioned as above, then tested with N=5 specimens per sample in a CEAST pendulum impact testing apparatus (Instron, Norwood, MA) with a 50N hammer. Multivariate ANOVA (analysis of variance) was performed to determine statistical differences in all properties tested between composite types. Waller-Duncan Post-hoc analysis in R from the "agricolae" package was used to compare significantly different subgroups of samples. After mechanical testing, failure surfaces from each type of testing were observed via SEM to examine the effect of CNF content on failure mode of composites.

Table 1: Formulations and relative weight percent of PLA, Wood Flour, CNFs, and LCNFs used in the manufacture of composites for mechanical testing.

| **Formulation** | **Wt.% PLA** | **Wt.% WF** | **Wt.% CNF** | **Wt.% LCNF** | **Composite Code** |
|---|---|---|---|---|---|
| Pure PLA | 100 | 0 | 0 | 0 | PLA |
| WF | 80 | 20 | 0 | 0 | PLA/WF |
| WF-10%CNF | 80 | 18 | 2 | 0 | 80/18/2 |
| WF-30%CNF | 80 | 14 | 6 | 0 | 80/14/6 |
| WF-50%CNF | 80 | 10 | 10 | 0 | 80/10/10 |
| WF-10%LCNF | 80 | 18 | 0 | 2 | 80/18/2L |
| WF-30%LCNF | 80 | 14 | 0 | 6 | 80/14/6L |
| WF-50%LCNF | 80 | 10 | 0 | 10 | 80/10/10L |
| SDCNF | 80 | 0 | 20 | 0 | PLA/SDCNF |

### 2.3.3. Water Removal and Energy Analysis

Three separate 100g samples of wet furnish at 5 wt.% from each formulation were weighed out, and moisture content was determined for each formulation to establish the starting mass of solids in the samples. Each sample was pressed at least five times using the same parameters as before, and the mass of the remaining material was recorded after each subsequent pressing event. Pure CNFs at 3% solids

were also pressed to provide a comparison. Paper towels under the mesh screens were replaced after each pressing event to prevent water pooling and re-absorption into the material through the mesh screens. The resulting solids after pressing were calculated by comparing the mass recovered to the starting solids of the material. The drying energy requirement per gram of dried CNF for each mixture was determined using a theoretical energy calculation based on the specific heat capacity of water (Equation 1), using the mass of water remaining after five pressing events.

$$q = mc\Delta T \qquad (1)$$

where q is the total heating energy in joules, m is the mass in grams, C is the heat capacity of water (4.186J/g*°C), and ΔT is the change in temperature. In this case, the change in temperature was the measured between ambient temperature (~25 °C) to the evaporation temperature of water (100 °C), hence ΔT = 75 °C. The latent heat of evaporation for water (2260 J/g) was then multiplied by the mass of water remaining, then added to the total heating energy from Equation 1 to obtain theoretical values for "drying energy." This was also done on pure CNF samples before and after pressing.

Hard to remove water (HRW) analysis was done in accordance with previous methods[16][26][27], where HRW content is determined from the drop in weight loss rate of water in an isothermal heating method above the boiling point of water but below the thermal degradation temperature of other components in the furnish. HRW is an indication of tightly bound water in a sample; less HRW content in a furnish can be correlated with less bound water in a sample, indicating less energy required to fully dry the sample. Here, an isothermal heating profile was used on a Thermogravimetric Analyzer (TGA) machine (TG500, TA Instruments, New Castle, DE), heating to 120 °C with a heating rate of 100 °C/min (~30 mg sample size) and maintaining the temperature at 120 °C for 15 minutes. Hard to remove water content (%/%) was calculated by measuring the total mass percent at the start of the time-dependent second derivative drop in mass, subtracting the final mass percent after drying had completed (percent solids of material), then dividing by the final mass percent (Equation 2). This was done for two samples of each wet furnish type, as well as WF in water at 5% solids and CNF/LCNF at 3% solids, with the results being reported in terms of averages of the two HRW results.

$$HRW\ (\%/\%) = \frac{(m_1 - m_2)}{m_2} \qquad (2)$$

where $m_1$ and $m_2$ are the mass % at the start of the 2nd derivative drop and the final solids of the material, respectively.

### 2.3.4. Dewatering Scale-Up

The dewatering process was scaled-up to determine if the energy efficiency seen in lab scale dewatering and drying could be replicated in a larger scale production environment while tracking energy use during the pressing, drying, and milling processes, as well as producing enough material for 50 lbs of a PLA/WF/CNF composite. WF-10%CNF was chosen for this purpose attributable to favorable tensile properties form mechanical testing. WF-10%CNF was mixed at 10 wt.% solids using the same methods as lab scale mixing for dewatering in a 12-quart Hobart batch mixer (Hobart Corp, Troy, OH). The target was 12.5 dry pounds (5.7 kg) of material (~125 lbs/56.8 kg wet). After mixing, the material was split into two batches (one batch 66.3lbs/30.0 kg and the other 58.7 lbs/26.7 kg). Each batch was placed between mesh screens and pressed 5 times in a 5' x 8' industrial cold press at UMaine ASCC in Orono, ME, targeting 300-500 psi pressure. Between press cycles, the press was opened, excess water sitting on the press was manually wiped away, and the furnish was weighed, mixed, and pressed again. Water removal and final solids were calculated as in Section 2.3.3, and the results of both batches were averaged together and compared to the wt.% solids per press cycle results from the lab-scale press. After pressing, the material was oven dried (VWR International 1600 HAFO Series, Radnor, PA) for 18 hrs. at 103 °C, and then ground in a pelletizing mill (U.S. screen size #12). A Fluke power meter (Everett, WA) was connected to the press, oven, and grinder to obtain power use (in kW) and time data for each step of the process. For the press, the power of each press event was multiplied by the time of each press event (hours) to obtain kWh units for energy, which was then summed together for each batch. Since oven power use changed over time based on the remaining moisture content of the material, the oven power consumption was averaged over three 6-hour intervals, the average power for each interval was multiplied by 6 hours, and the resulting energy use was summed together (Figure 2). The grinder energy use was

measured similarly to the press, with the power spikes corresponding to grinder turning on multiplied by time and summed together. These results were converted into kJ, then compared to empirical data for the energy required to produce SDNCF obtained from Oak Ridge National Laboratories. To provide a basis for comparison, the energy results were normalized by gram of dry CNFs produced by each process.

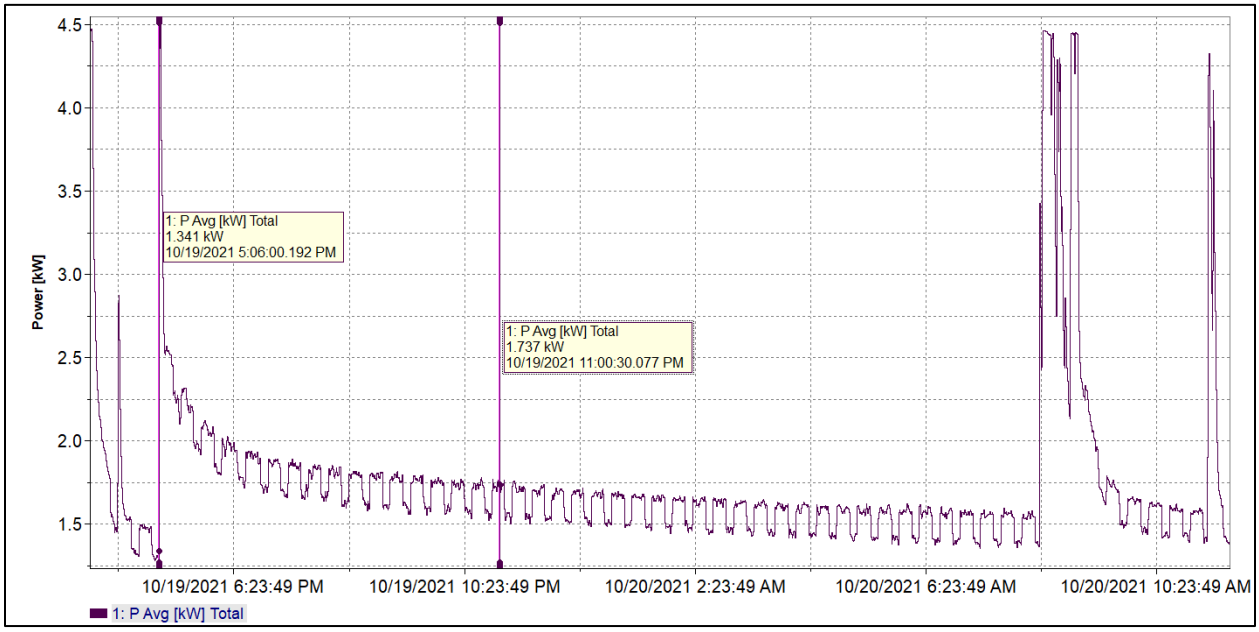


Figure 2: Power consumption (kW) over time data obtained from the power logging software. Vertical bars at t=0 (~5:00PM) and t=6hrs. (~11:00PM) show how time was divided into intervals for average energy use calculations.

To provide smaller dimensions of PLA for compounding with the furnish, PLA powder was obtained by shipping PLA pellets to Advanced Cryogenic Enterprises (Akron, OH), where they were cryo-milled with an 80 mesh filter and sent back to the UMaine Advanced Structures and Composites Center for compounding. The powder was used to better match the size of WF-CNF furnish during compounding and reduce shape incompatibility during compounding. The resulting powder and dewatered/dried/milled WF-10%CNF furnish were conditioned for at least 4 hours (50-55 ℃ for PLA and 100-103 ℃ for the furnish, respectively). The PLA powder was conditioned at lower temperatures than the larger pellets as higher temperatures caused the smaller particles to fuse together during the conditioning process. After conditioning, the powder and furnish were compounded together in a Brabender co-rotating twin-screw extruder (Brabender, South Hackensack, NJ) at 230 ℃ with a screw

speed of 110 rpm. The loading zone of the extruder was set to 160 ℃ so that the fine powdered PLA would not sinter together before being pulled into the screws and cause issues with homogeneity of the shear-mixed material. After compounding, the final 80/18/2 %PLA/WF/CNF composite was pelletized (U.S. screen size #6) and provided to ASCC personnel for printing test samples on a Gigabot X 3D Printer (re:3D Inc, Houston, Texas). The test prints were rectangular, with 101.6 x 50.8 x 50.8 $mm^3$ dimensions. For printing, a 21 mm bead width and 0.8 mm layer height were used. Heat zone 0 was set to 190 °C, zone 1 to 180 °C, and zone 2 to 170 °C. The bed temperature was 45 °C, the print speed was 15 mm/s, and the nozzle size was 1.75 mm.

## 2.4. Results and Discussion

### 2.4.1. Furnish Manufacture and Characterization

The addition of CNFs to WF induced changes in the distribution of particle sizes within furnishes (Figure 3). The distribution of particle major axes or lengths in the unmodified WF furnish after milling was relatively broad staying below 1.2 mm, but the addition of even 10 wt.% CNFs to wood particles induced a strong positive skew to the length distribution, heavily favoring particle lengths below 0.6 mm, with a strong peak below 0.2 mm. CNF addition at 30 and 50 wt.% added even more positive skew, with a drastic jump in skewness at 50 wt.%, which appears to slightly broaden the distribution below 0.4 mm. While it is expected that CNF attachment to WF particles may increase the particle sizes, the more positively skewed distributions indicate smaller particle sizes with higher CNF addition. This may be attributable to smaller pieces of dry CNFs being sheared off WF during the milling process. The skew did not change as drastically with increasing LCNF addition, possibly because of the lower stiffness of LCNF from OCC due to the presence of lignin and other impurities preventing it from breaking into smaller particles[28].

CNF addition also added a slight positive skew to the distribution of particle aspect ratios (Figure 25), with the strongest skew seen at 50 wt.% CNF addition and an increase in peak frequency toward the lower end of the distribution. Similar to length distributions of WF-LCNFs, no strong trend in aspect ratio

change was seen with increasing LCNF addition, with WF-50% LCNFs actually showing a less positive skew than WF despite having stronger peaks at the lower end of the distribution (between 1.3 mm and 2.0 mm). Despite the high standard deviations and coefficients of variation, ANOVA testing showed significantly lower aspect ratios at higher levels of CNF/LCNF substitution, with pure WF having a significantly higher average aspect ratio than all furnishes with CNFs/LCNFs, and each subsequent increase in CNF substitution having a significantly lower aspect ratio than the previous weight % substitution. The exception to this was WF-30%LCNF and WF-50%LCNF formulations, where WF-50%LCNF sample had a significantly higher average aspect ratio than WF-30%LCNF. The average major axis dimension of WF was also significantly higher than all subsequent CNF/LCNF additions, but WF-CNFs did not see a significant change in major axis dimension until WF-50%CNF. The WF-10%LCNF formulation had a significantly higher major axis dimension than both WF-30% and WF-50%LCNF, which were not significantly different. Overall, the addition of higher levels of CNF and LCNF onto WF seem to reliably decrease major axis dimensions and aspect ratios of furnishes, although the high variation indicates that large sample sizes are required to see this change. Shapiro-Wilk and Kolmogorov-Smirnov tests did not reject normality of the datasets (all groups had $P>0.05$ for both measurements).

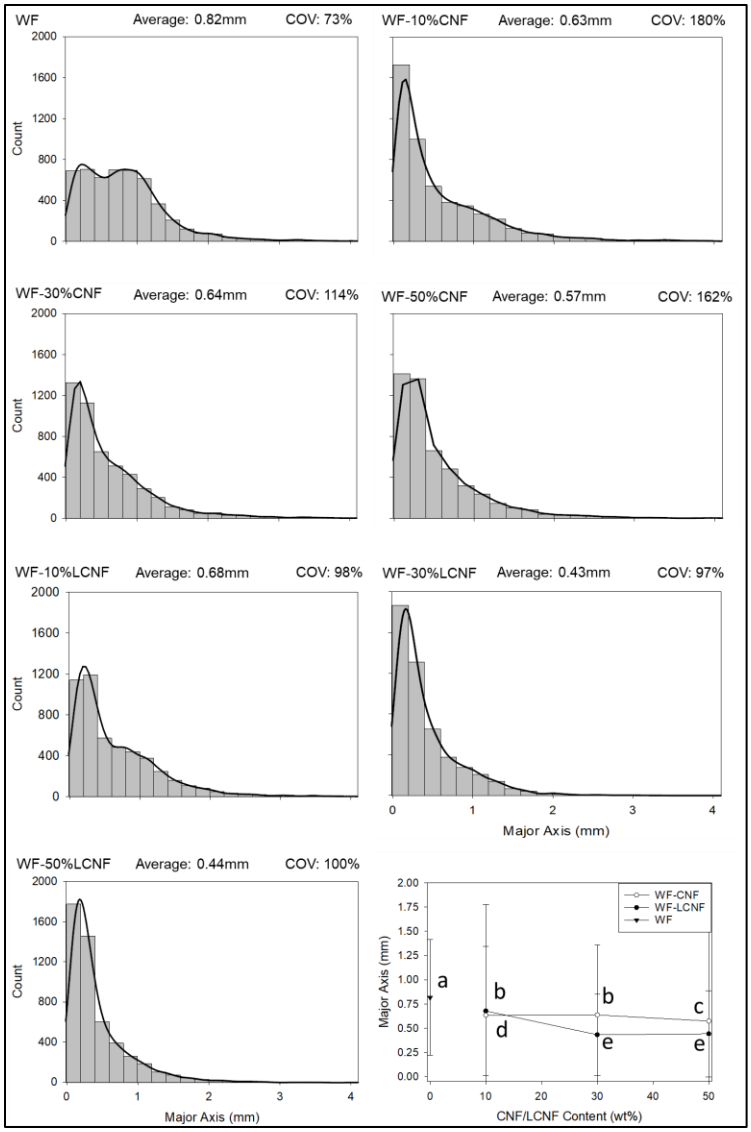


Figure 3: Histograms of major axis dimensions (bin size = 0.2 mm) from particle size analysis with kernel density overlays, (bandwidth = 9.23*10-2) and comparison of average major axis lengths for each furnish. Common letters on data points on the average comparison graph indicate statistically insignificant differences at 95% confidence level. Error bars are based on sample standard deviation from the mean.

As seen in the SEM images comparing dewatered WF-CNF furnishes to WF and SDCNF (Figure 4 for CNF, Figure 26 for LCNF), CNF and LCNF appear to preferentially attach to WF, and do not become separated during the drying or milling processes. The WF-10% and WF-30%CNF furnishes show minor structures of CNFs attached to WF, whereas the WF-50%CNF furnish shows a heavy coating of CNFs on the WF surface. This is evidenced by the higher charging, which increases with levels of

insulating CNF on the sample during SEM imaging[29]. The higher levels of CNF prevent electrons from properly conducting out of the sample, causing the charging effect. All WF-CNF and WF-LCNF hybrid furnishes showed evidence of nanofibrillar CNFs/LCNFs preserved on the surfaces of WF, while WF-LCNF surfaces seem to be slightly more dominated by an agglomerated form of LCNF with diameters larger than 1µm. While SDCNF exhibited micron-sized pieces of dried CNF, very few nanofibrillar dimensions appear to be preserved, indicating that our dewatering and drying process may reduce agglomeration of CNF compared to the spray drying process. The smaller particles seen in the 30x SEM of WF-CNF furnishes may have contributed to the positively skewed length distributions seen in Figure 2, and appear to be mostly pieces of WF with some CNF attached. This could be because of the strong interfacial compatibility between the wood particles and CNF, as well as the inherent strength and stiffness of CNF, causing larger WF-CNF particles to break with a wood failure mechanism as opposed to CNF being removed from the surface of the wood particle.

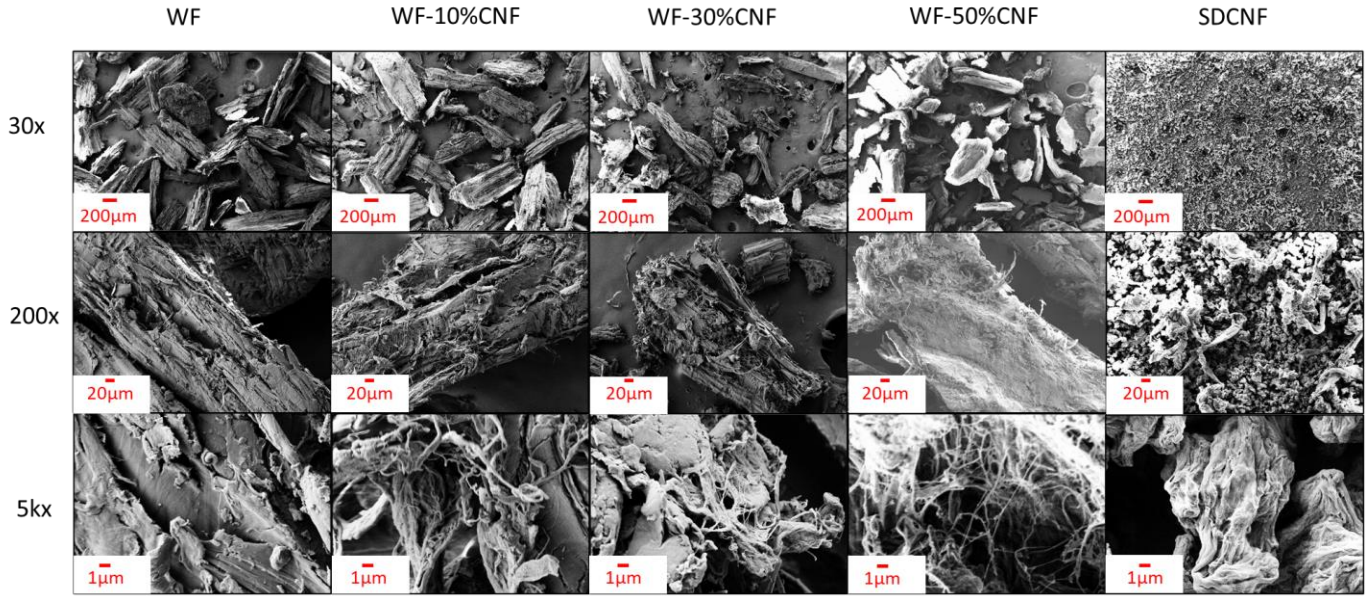


Figure 4: SEM Images of WF, WF-10%CNF, WF-30%CNF, WF-50%CNF and SDCNF samples. Top to bottom: 30x, 200x, 5kx magnification.

### 2.4.2. Composite Processing and Testing

As shown in Figure 5, low levels of CNF/LCNF (2 wt.% and 6 wt.%) addition appear to reduce the flexural strength of the composite compared to PLA and PLA/WF, while maintaining a similar flexural modulus to PLA/WF. These lower levels of addition also appear to have high standard deviations, indicating the possibility of poor or overly heterogeneous dispersion of material within the matrix. At 10% CNF/LCNF addition, the flexural strength was more comparable to PLA/WF, PLA, and PLA/SDCNF, with a slight reduction in flexural modulus compared to lower levels of CNF/LCNF addition and PLA/WF. The standard deviation also appears to shrink compared to the lower levels of CNF/LCNF addition. LCNF imparted better flexural properties than CNF, possibly attributable to a compatibilizing effect of lignin[19] and lower relative cellulose content, but these gains were not considered statistically significant. Strain at break slightly increased with higher LCNF/CNF addition, which could be considered an inverse effect of the decreasing stiffness of the material, as a lower stiffness could result in higher ductility. The "best performing" hybrid composites with 10% CNFs and LCNFs had comparable flexural strength to PLA/20%SDCNF, with a significantly flexural higher modulus, indicating the practicality of using this method for incorporating CNFs into composites over SDCNF.

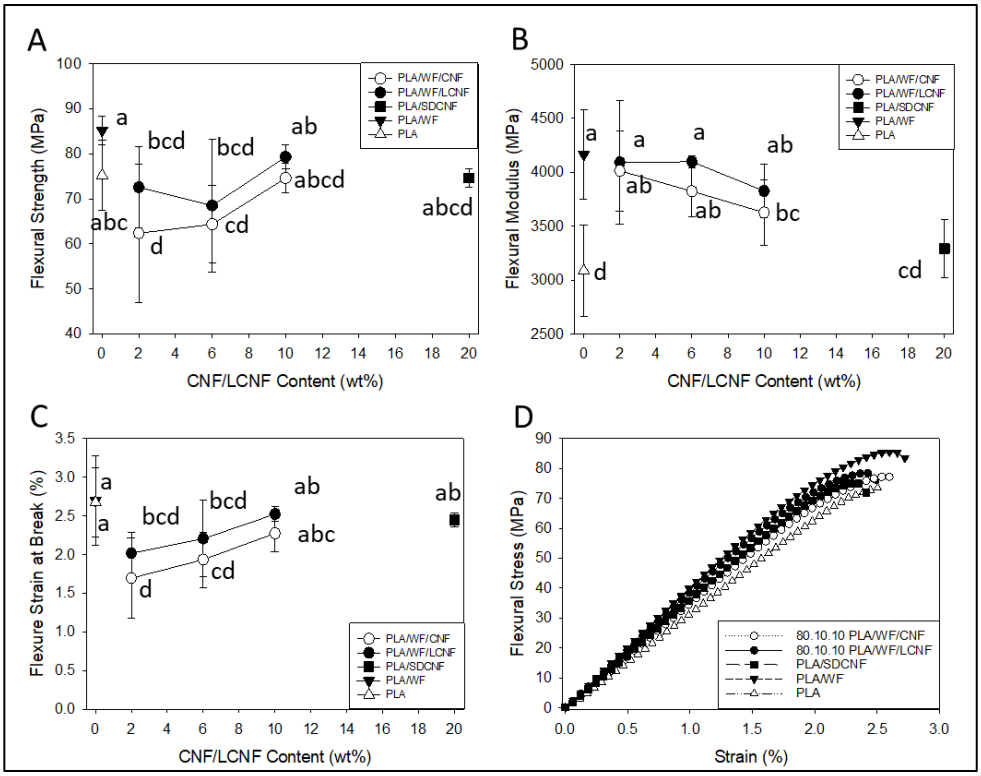


Figure 5: Flexural testing results from PLA/WF/CNF and PLA/WF/LCNF hybrid composites, compared with PLA, PLA/WF, and PLA/SDCNF results. (A) Flexural strength, (B) flexural modulus, (C) flexural strain at break, and (D) typical stress/strain curves from flexural testing. Common letters on data points indicate statistically insignificant differences at 95% confidence level.

In Figure 6, tensile strength results show an inverse relationship compared to flexural strength, with 2wt.% CNF/LCNF showing higher strength values than composites with higher CNF/LCNF contents. Like flexural modulus, tensile modulus also decreased with increasing CNF/LCNF content, likely because of a relatively lower wt.% of higher aspect ratio maple wood particles in the composite. The 2 wt.% CNF/LCNF additions did, however, significantly increased the tensile modulus of the material compared to PLA/WF. Unlike the flexural testing results, LCNF hybrid composites had much poorer tensile strength performance than CNF hybrid composites, potentially owing to the low tensile strength of lignin [28][30]. High standard deviations are still seen in 2-6 wt.% CNF/LCNF hybrid composites, potentially confirming poorly dispersed/highly heterogeneous particles. CNFs/LCNFs did not significantly affect tensile strain at break compared to PLA/WF, with PLA and PLA/SDCNF showing

much higher levels of elongation than PLA/WF composites. The higher strain at break for PLA/SDCNF is possibly attributable to greater homogeneity of the furnish, which may have improved its dispersion., while higher aspect ratio WF particles act as reinforcing materials that increase modulus while reducing ductility. This could be attributed to poor fiber/matrix interaction, and the wood fibers may have inhibited polymer chain mobility[31]. Similar experiments with PP/SDCNF composites showed that SDCNF had relatively minor effects on viscosity[32], meaning it may have less of an effect on polymer chain mobility than the higher aspect ratio WF.

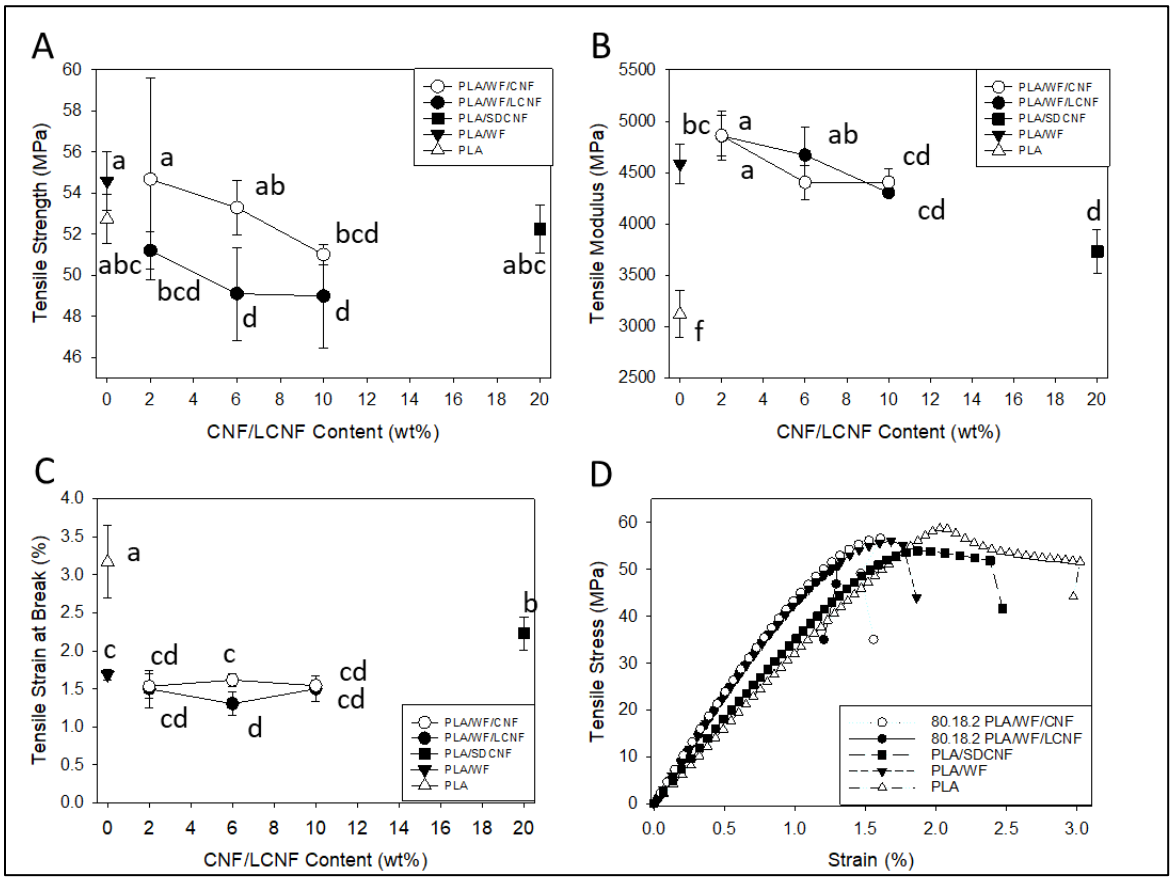


Figure 6: Tensile testing results from PLA/WF/CNF and PLA/WF/LCNF hybrid composites, compared with PLA, PLA/WF, and PLA/SDCNF results. (A) Tensile stress at break, (B) tensile modulus, (C) tensile strain at break, and (D) example stress/strain curves from tensile testing. See Figure 5 for an explanation of letters.

SEM Analysis of tensile fracture surfaces (Figure 7) shows the presence of some fibrillar morphologies in all CNF composites after compounding and testing, along with larger scale CNF agglomerates that appear to have been separated from WF. It is unknown whether this separation occurred

during the compounding process or testing; slip between WF/CNF or PLA/CNF interacting phases may contribute to the higher variation in hybrid composite results, and potentially the lower tensile strengths at higher levels of CNF addition. The composite fracture surfaces seem to become overall "rougher" with higher levels of CNF addition, indicating greater heterogeneity in furnish morphology.

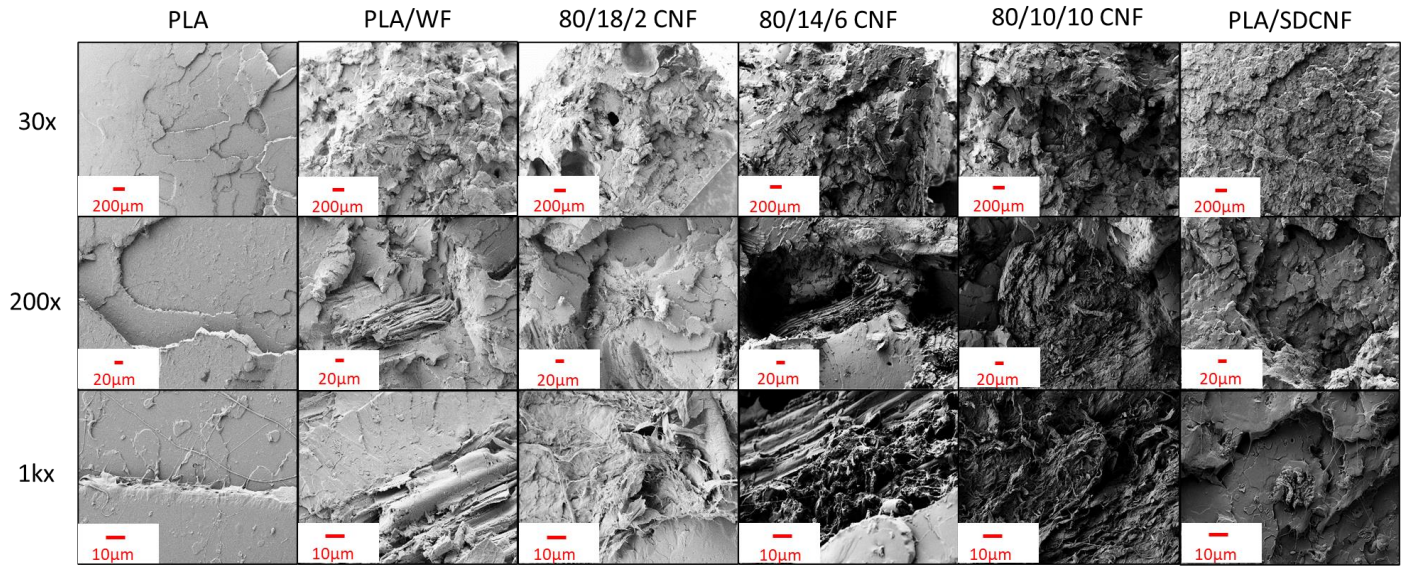


Figure 7: SEM images of tensile fracture surfaces from PLA/WF/CNF composites. Top to bottom: 30x, 200x, 5kx magnification. Sample codes follow PLA content/WF content/CNF content (wt.%) convention.

To better understand the efficacy of this hybrid composite method compared to using only SDCNF, tensile, flexural, and impact properties from testing were compiled into a table, along with the respective % improvement (+) or drop (-) in each property compared to the PLA/SDCNF composite as a reference (Table 2). Overall, the hybrid composites had much higher modulus values compared to PLA/SDCNF, likely owing to the presence of WF, making them more practical for applications where material stiffness is required. The hybrid composites also had overall comparable tensile strength to PLA/SDCNF, but lower levels of CNF in hybrid composites showed large decreases in flexural and impact strength compared to PLA/SDCNF. The 10 wt.% CNF/LCNF hybrid composites had more favorable or comparable flexural and impact strengths to PLA/SDCNF. Since impact strength is often inversely correlated with material stiffness and brittleness, and the 10wt.% CNF composites showed

lower moduli and higher flexural strain at break values than all other hybrid composites, this is not unexpected. Since impact testing specimens were made from broken flexural test specimens, residual stresses may have reduced overall material toughness. Despite this, the difference in impact strength between sample groups shows that CNF addition to furnishes likely influences composite impact strength. Overall, the comparable strengths and much higher moduli of the 10 wt.% CNF composite indicate its practicality over SDCNF in PLA reinforcement applications.

Table 2: Summary of average composite properties (with standard deviations) from tensile, and notched IZOD impact testing, as well as percent improvement or loss as compared to composite with 20wt.% SDCNF for each property. Refer to Table 1 for composite codes.

| **Composite** | **Tensile** | | | | **Flexural** | | | | **Impact** | |
|---|---|---|---|---|---|---|---|---|---|---|
| | **Strength (MPa)** | **% SDCNF** | **Modulus (GPa)** | **% SDCNF** | **Strength (MPa)** | **% SDCNF** | **Modulus (GPa)** | **% SDCNF** | **Strength (J/m)** | **% SDCNF** |
| PLA | 52.7 ± 1.2 | +0.8 | 3.12 ± 0.23 | -16.4 | 75.2 ± 7.7 | +0.8 | 3.09 ± 0.42 | -6.4 | 28.1 ± 2.6 | -3.1 |
| PLA/WF | 54.6 ± 1.4 | +4.5 | 4.58 ± 0.19 | +22.9 | 85.2 ± 3.2 | +14.2 | 4.16 ± 0.41 | +26.4 | 25.4 ± 2.9 | -12.5 |
| 80/18/2 | 54.7 ± 4.9 | +4.6 | 4.86 ± 0.20 | +30.3 | 62.3 ± 15.4 | -16.4 | 4.01 ± 0.37 | +21.9 | 20.4 ± 5.0 | -29.7 |
| 80/14/6 | 53.3 ± 1.3 | +2.0 | 4.40 ± 0.16 | +18.0 | 64.3 ± 8.7 | -13.7 | 3.82 ± 0.24 | +16.2 | 20.1 ± 2.5 | -30.7 |
| 80/10/10 | 51.0 ± 0.5 | -2.4 | 4.41 ± 0.13 | +18.1 | 74.6 ± 3.3 | 0.0 | 3.63 ± 0.31 | +10.1 | 30.3 ± 3.5 | +4.4 |
| 80/18/2L | 51.2 ± 0.91 | -2.0 | 4.86 ± 0.24 | +30.2 | 72.5 ± 9.1 | -2.7 | 4.09 ± 0.57 | +24.3 | 22.3 ± 6.2 | -23.1 |
| 80/14/6L | 49.1 ± 2.3 | -6.0 | 4.67 ± 0.27 | +25.2 | 68.5 ± 14.8 | -8.2 | 4.10 ± 0.06 | +24.5 | 19.4 ± 4.6 | -33.0 |
| 80/10/10L | 49.0 ± 2.5 | -6.2 | 4.30 ± 0.05 | +15.4 | 79.3 ± 2.7 | +6.3 | 3.83 ± 0.25 | +16.2 | 27.4 ± 2.0 | -5.4 |
| PLA/SDCNF | 52.3 ± 1.2 | N/A | 3.73 ± 0.22 | N/A | 74.6 ± 2.0 | N/A | 3.3 ± 0.27 | N/A | 29.0 ± 2.7 | N/A |

### 2.4.3. Water Removal and Energy Analysis

HR water determination of furnishes (Figure 8) show that the addition of WF to CNFs and LCNFs drastically reduces the HR water content of the material compared to pure CNFs/LCNFs. Even the 50-50 mixes of WF-CNFs and WF-LCNFs showed comparable results to WF in water at 5% solids content, indicating the efficiency of WF in providing an energetic transfer of bound water to free water in the system. These results are consistent with those of a previous study where HR water of WF-CNFs was determined at 3% total mixture solids and 30%CNF content[16], showing that the reduction in HR water content may be more a function of wood particle addition than starting solids. This reduction by wood particle addition may reduce the overall energy consumption required to dry the material, as the relative ratio of bound water in the system is drastically reduced by even 50% wood particle addition. It may be worth exploring the effect of smaller levels of wood particle addition on HR water content to facilitate drying, even if CNF-CNF interactions and agglomeration are more likely with less WF. Although LCNFs before the addition of WF appear to have higher general HR water values than CNFs, values for hybrid furnishes seem to be comparable. This indicates that WF is likely very efficient at reducing the bound water content of CNF regardless of the interfacial characteristics of non-CNF impurities in the system.

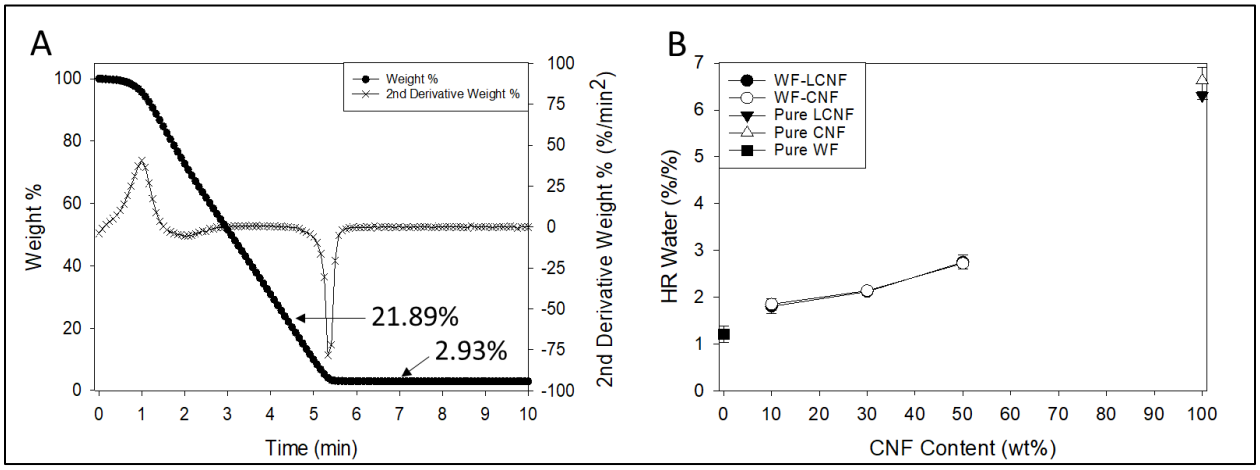


Figure 8: (A) TGA curves for HR water determination of CNF at ~3% solids content. 21.89% is the weight % of the material at the start of the changing water evaporation rate, indicated by the drop in the 2nd derivative weight curve. 2.93%

represents the final solids of the material. (B) HR water contents of WF-CNF and WF-LCNF Furnishes (CNFs and LCNFs at ~3% solids, all other furnishes at ~5% solids).

As seen in Figure 9, water removal shown by final wt.% solids (extrapolated from starting moisture content and mass of pressed furnish) of pressed wet furnishes seems to follow a polynomial relationship with number of presses ($R^2$ = 0.98 - 0.99), which begins to asymptote for most furnishes around 60-70 wt.% solids. Water removal seemed to occur more quickly in LCNF furnishes than in CNF ones, with significantly different LCNF group solids values from CNF group solids values at 5x presses (p-value = 6×10-5, p-value < 0.05). This faster water removal in WF-LCNF formulation may be associated with the higher lignin, hemicellulose, and assorted hydrophobic small molecule content facilitating the conversion of bound water in LCNF to free water, because of the lower affinity of LCNF for water compared to CNF or slightly lower HR water content on LCNF (Figure 8). Water removal also seems to drop slightly with higher CNF content, potentially owing to the higher proportion of bound water content in CNF to free water in the system. Theoretical energy required to dry the system per gram of "dry" CNF seems to drop drastically after 5 presses, from

81 kJ for 3% solids CNF to 17 kJ for pressed WF-10%CNF. Because of the higher CNF content and similar level of water removal, 50wt.% CNF and LCNF have even lower drying energy requirements per g of dry CNF, comparable to pressed CNF. WF-CNF/LCNF had higher ease of handling during dewatering than pure CNF, as the shear thinning behavior of pure CNF[33] meant that material was more easily lost from the sides of the press during the dewatering process. The addition of wood fibers likely increased the viscosity of the mixture and reduced its shear thinning properties attributable to the increase in viscoelastic solids content, although a full rheological characterization of these systems is yet to be performed. The favorable drying energy, presence of nanoscale dimensions after drying, and ease of handling of these systems compared to pure CNF have positive implications for scaling up CNF drying processes using contact dewatering methods. Practical methods involve actual measurement of energy use during drying, such as energy required for larger mechanical presses, ovens, and grinders, and should be

explored before further conclusions are made about the practicality of drying these systems, even if the theoretical energy consumption values appear to be favorable.

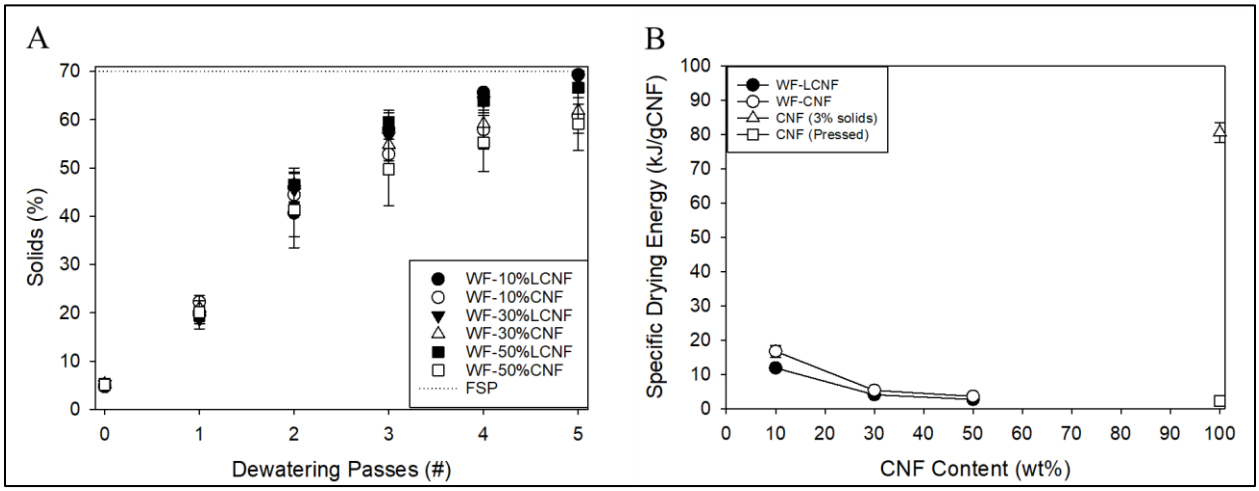


Figure 9: (A) Percent solids of furnishes after multiple dewatering passes. (B) Theoretical drying energy calculated for furnishes after 5x dewatering passes compared to 3% solids CNF and pressed CNF.

### 2.4.4. Dewatering Scale-Up

Dewatering was successfully scaled up to accommodate 125 lbs/56.8 kg of wet WF-CNF furnish. After pressing 5 times, an average final solids content of 49.3 wt.% was achieved for WF-10%CNF in the large-scale press (Figure 10A). Though the starting solids (10 wt.%) was higher than at the lab scale (5 wt.%), this was lower than the solids achieved for WF-10%CNF at the lab scale after 5 presses (60.7 wt.% solids). This is likely attributable to the larger mass of material and therefore surface area occupied in the press dissipating pressure from pressing and preventing the movement of water out of the material, and the lack of water removal during the press event, such as the use of paper towels under the mesh screen for the lab-scale press. The solids content begins to asymptote around 45-50 wt.% for the large-scale press after 3 cycles, indicating that the press method begins to have diminishing returns for dewatering material at this point.

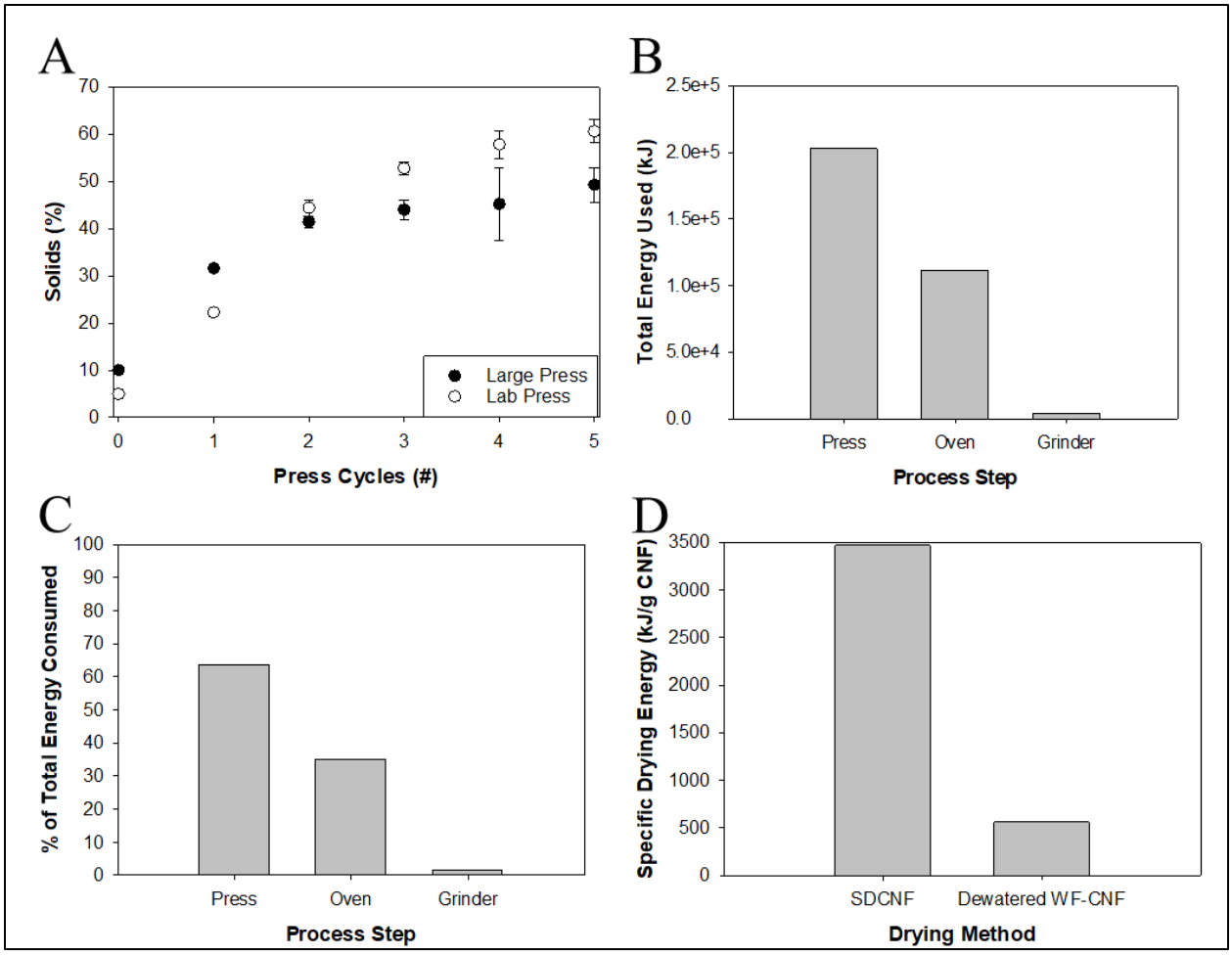


Figure 10: Summaries of results from WF-CNF scale-up dewatering process. (A) Percent solids of furnishes after multiple dewatering passes, with comparison between scaled-up results and lab results. (B) Total Energy (kJ) used for each step in scaled-up dewatering process. (C) % of total energy used by each step in the scaled-up dewatering process. (D) Specific drying energy per gram of dry CNF comparison between ORNL SDCNF drying process and scaled-up CNF dewatering/drying process.

The pressing of the material was the most energy-intensive step of the dewatering process (Figure 10B and 10C), accounting for 63.6% of the total power consumption of the process compared to 35% and 1.4% for the oven drying and grinder, respectively. The potential exists for the press power to be optimized by removing excess water during each press cycle, using a larger press to press more material at once, and only pressing until diminishing returns in water removal are seen (~3 presses as opposed to 5). The total power consumption from this process was $3.19*10^5$ kJ, which was normalized to specific drying energies of 56.17 kJ/g of dry furnish and 561.7 kJ/g of dry CNFs. Compared to the values obtained

for the ORNL spray drying process (3465.2 kJ/g dry CNFs), this is a 6-fold or 84% decrease in the total energy required to produce dry CNFs (Figure 10D). This also showed a 33-fold increase in the values obtained from theoretical lab-scale calculations (17 kJ/g). The final PLA/WF/CNF composite pellets produced from this were successfully 3D printed into 101.6 x 50.8 x 50.8 $mm^3$ test samples (Figure 11) showing the viability of this method to produce 3D printed PLA composites with CNF.

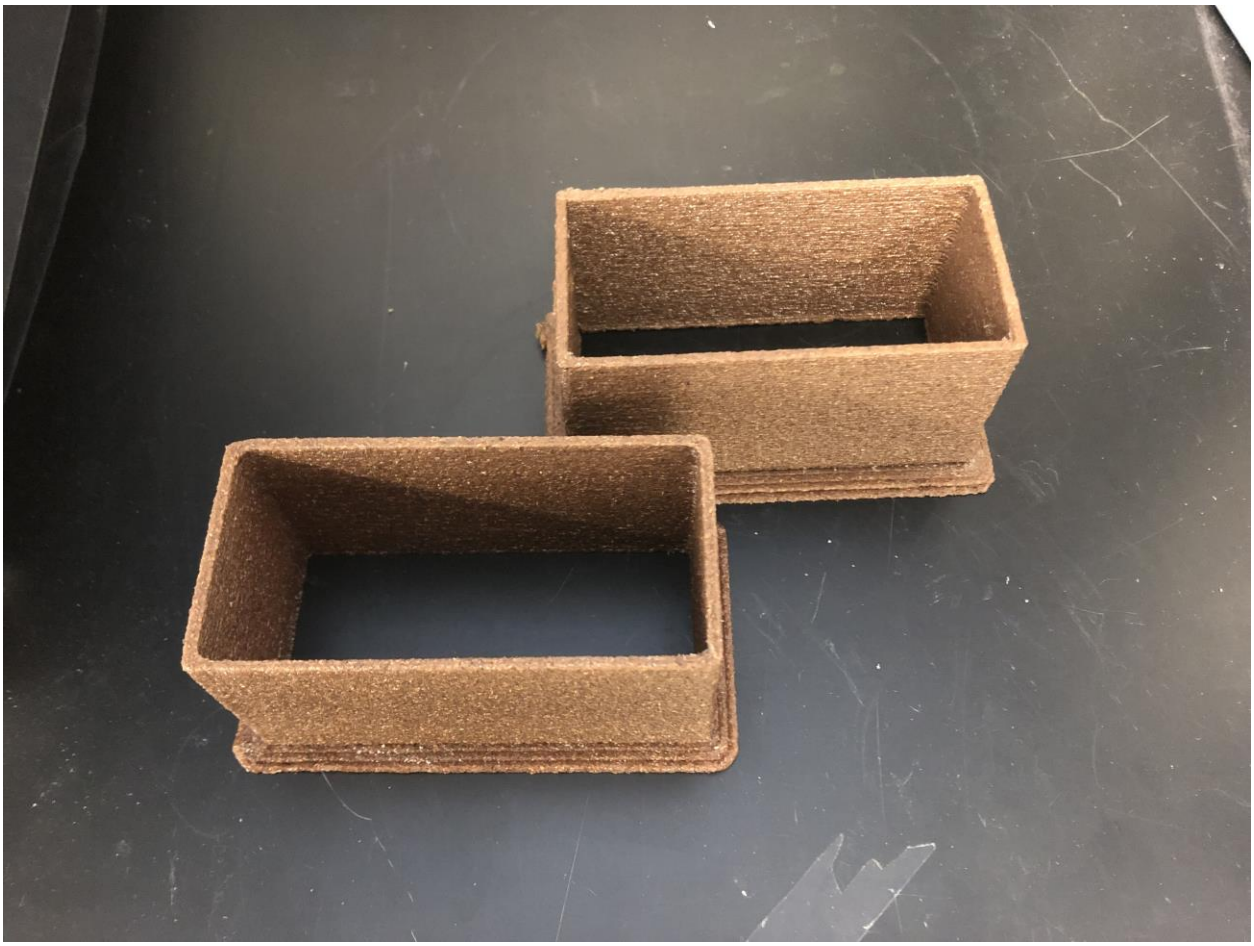

Figure 11: 3D printed test samples from scaled-up PLA/WF/CNF composite manufacture.

## 2.5. Conclusions

The viability of contact dewatered WF-CNFs and WF-LCNFs as means of producing dried CNFs for hybrid composite systems with PLA has been explored, with mixed-to-favorable results. While evidence of nanoscale dimensions of CNF was demonstrated in these systems, these did not seem to translate to

significant improvements in mechanical strength compared to pure PLA, PLA with unmodified WF, or PLA with SDCNF. The comparable flexural and tensile strengths of these systems, however, were achieved at potentially much lower drying energy requirements, contributing to the economic and "green" nature of this process. The moduli of the hybrid composite systems were much higher than PLA or PLA/SDCNF, while retaining comparable moduli to PLA/WF, showing some promise in composite applications. Further explorations should be performed in these systems at lower (<2 wt.%) and higher (>10 wt.%) CNF/LCNF additions to better understand the effect of CNF/LCNF content on mechanical performance in these systems, as well as morphological differences in dry CNFs/LCNFs based on WF:CNF/WF:LCNF ratios. The relative ease of drying these systems while preserving nanoscale dimensions, however, does show favorable results compared to pure CNFs, which will otherwise dry in the form of large-scale agglomerates that are difficult to incorporate into composites. Overall, these hybrid composite systems show some promise, but should be further explored in terms of optimizing the preservation of nanoscale morphology and final composite strength and stiffness. When the dewatering process was scaled up, an 84% decrease in specific drying energy for CNFs was observed compared to an industrial spray-drying method. This, along with the nanofibril dimensions observed after drying, indicate that this process may be a more-cost efficient way of producing dry nanoscale CNFs than spray drying.

# CHAPTER 3

# DEWATERING OF CNF WITH PLA POWDER FOR PLA/CNF COMPOSITES

## 3.1. Chapter summary

Cryocrushed PLA powder was mixed with CNF suspensions to facilitate dewatering via mechanical pressing. The dewatered materials were oven dried, ground, characterized, processed, mechanically tested, and analyzed for water removal and energy efficiency similarly to WF-CNF furnishes in Chapter 2. After creating masterbatches of PLA-CNF composites and testing, unfavorable mechanical properties were observed with CNF addition, and agglomerated CNF morphology observed in polarized light microscopy drove the decision to lower the CNF loading for dewatered composites. The lower CNF levels were tested as before, and hot-pressed films of dewatered PLA-CNF underwent tensile testing as a first-pass method to show CNF composite reinforcement potential before larger shear-mixed samples were made and tested. Masterbatch samples showed high levels of CNF agglomeration, while lower levels of CNF showed significant improvements in dry fibril morphology in the final composite as confirmed by PLM. The lower CNF levels showed significant improvement in tensile properties of PLA-CNF films compared to pure PLA up to the level at which agglomeration was observed within the films, with similar tensile strengths and higher tensile moduli than PLA composites with SDCNF in shear-mixed samples.

## 3.2. Introduction

Because of potential interfacial issues caused by loading hybrid WF-CNF furnish into PLA composites shown above, the effect of directly dewatering CNF with PLA particles was examined. Numerous previous methods have explored PLA-CNF nanocomposites, including solvent-exchanging or acetylating CNFs mixing with dissolved PLA[34][35], or mixing PLA with SDCNFs[36]. This method was inspired by polymer latex processing of CNF, wherein polymer latex micelles in an aqueous suspension separate and “trap” CNF fibrils during solvent removal, preventing them from agglomerating and aiding dispersion[37][38]. This method has not been explored using solid thermoplastic PLA to facilitate the

removal of water of CNF suspensions, and to determine if this CNF trapping effect can be replicated to preserve CNF fibril dimensions after drying for non-latex suspensions. The goal was to obtain a direct processing method for drying and incorporating CNFs into functional PLA-CNF nanocomposites without the use of noxious solvents, spray-drying methods, or compatibilizers. Calculations to determine the minimum level of CNF to produce a monolayer to cover all PLA particles in a mixture are included to understand how to optimize the system to produce small-scale CNFs attached to the surface of PLA.

## 3.3. Materials and Methods

### 3.3.1. Material Manufacture and Characterization

Cellulose Nanofibrils (90% fines, ~3 wt.% solids)) made from bleached softwood kraft pulp were sourced from the UMaine Process Development Center. PLA pellets (Natureworks Ingeo 4043D, Minnetonka, MN) were shipped to Advanced Cryogenic Enterprises (Akron, OH) and cryo-milled with an 80-mesh filter.

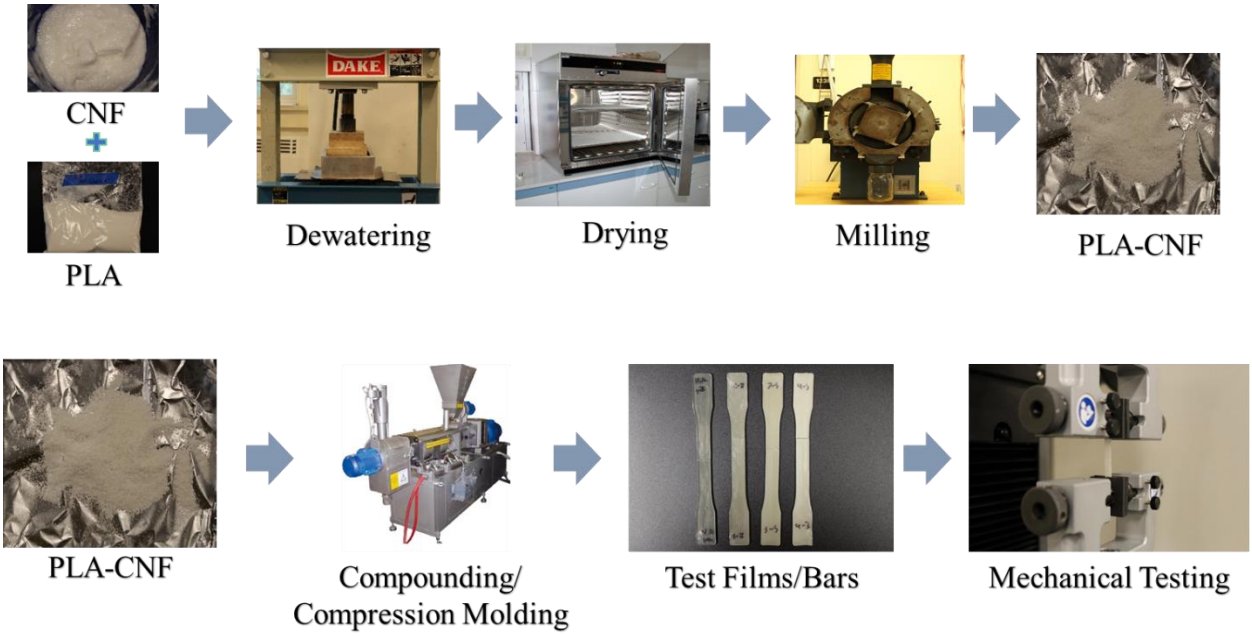


Figure 12: Outline for overall CNF dewatering with PLA process, as well as composite manufacture process.

The overall furnish preparation process is summarized in Figure 12. CNFs were mixed with PLA at different percent CNF contents (10, 30, 50 wt.%), targeting 5% total solids per mixture. First, the calculated amount of water was added to the CNFs, then PLA powder was added and mixed with the

suspension. The entire wet furnish was blended by a KitchenAid Artisan 5 stand mixer (St. Joseph, MI) at power setting 1 for 3 min. Approximately 1 g of each freshly mixed sample was analyzed with a moisture content analyzer to determine starting percent solids content, and 100-150 g of each mixture at a time was dewatered via cold pressing with a DAKE (Grand Haven, MI) hydraulic press. A square mold was used to contain the material, which was pressed at ~2.2 MPa (63.5 $in^2$ press area). Mesh screens were placed underneath the pressing area and on top of the furnish in the mold in order to evenly distribute pressure and ensure water removal, and paper towels were placed underneath the bottom mesh to prevent pooling and re-absorption of removed water. At lower CNF contents for film manufacture, PLA-CNF mixtures were made at 0.1, 0.5, 1, 2, 6, and 10 wt.% CNF, and mixed with a JJ-1 Precise Strength Power Mixer (VWR, Radnor, PA) and pressed as above targeting 20 wt.% initial mix solids. This was repeated to manufacture larger amounts of PLA-CNF at 0.5, 1, and 2 wt.% for the dewatered shear-mixed formulations.

The initial PLA-CNF dewatered compositions (10-50 wt.% CNF at 5 wt.% initial mix solids) were broken up into smaller wet pellets by the KitchenAid mixer (power setting 2, 3 min), then dried in a Fisherbrand Isotherm oven (Fischer Scientific, Waltham, MA) at 50 ℃ for 16 hours. For PLA-CNF dewatered at 20 wt.% solids (0.5-2 wt.% CNF), the dewatered cake was transferred directly from the press to the oven and dried at 50 ℃ for 16 hours while trying to keep the cake structure as preserved as possible. Dried samples were then homogenized in a Wiley Mill (Thomas Scientific, Swedesboro, NJ) utilizing a mesh sieve screen with 1 mm openings. To determine the difference in diameter between PLA powder and dry PLA-CNF mixtures, sieve analysis was performed (Retsch, Newtown, PA) using sieve pans with 500, 425, 250, 180, and 150 μm opening sizes. Sieve pans were weighed, then 10 g of each mixture was sieved with an amplitude of 1 for 20 minutes, after which pans were weighed again, and particle mass for each sieve size was determined by subtracting the empty pan mass from the sieved pan mass. The mass percent of each fraction size was determined by dividing the particle mass for each sieve size by the total collected particle mass of the mixture. Samples of all homogenized compositions were visualized at the nanoscale with scanning electron microscopy (SEM) to observe nanoscale structure of

dewatered CNF bound to PLA. For SEM, samples were dispersed on top of carbon-tape coated SEM stages, after which they were sputter coated with 4 nm of a gold/palladium material to provide a conductive layer over the samples. The SEM used was a Zeiss Nvision 40 (Oberkochen, Germany) at 3kV Electron High Tension.

### 3.3.2. Composite Processing and Testing

SDCNFs (90% fines) were produced from a 3 wt.% CNF slurry diluted down to 1 wt.% solids, which was then dried at 125°C with a 30,000 rpm atomizer. PLA-50wt.%CNF his was used as a masterbatch to manufacture PLA-10/20/30wt.%CNF mixtures by adding extra PLA powder to dilute down to the desired CNF wt.%. The masterbatched materials were conditioned for at least 4 hours at 50-55 ℃ before compounding via a Brabender counter-rotating twin-screw extruder (Brabender, South Hackensack, NJ) at 230 ℃ with a screw speed of 60 rpm. The loading zone of the extruder was set to 160 ℃ so that the fine powdered PLA would not sinter together before being pulled into the screws and cause issues with homogeneity of the shear-mixed material. A control was made with powder PLA only. The lower-level PLA-CNF compositions (0.5-2wt.%CNF dewatered at 20wt.%solids) were conditioned under the same parameters of the masterbatched samples, and were compounded in a smaller Brabender 30CC Half Size Mixer (Brabender, South Hackensack, NJ) at 175 ℃ with mixing elements set to 60 rpm. To manufacture PLA-SDCNF composites, SDCNFs and PLA powder were conditioned similarly to the previous mixtures before compounding, then hand mixed at the same CNF loading levels as the low-level CNF compositions.

All shear mixed composites (masterbatched, low-level CNF) were pelletized in a granulating mill (U.S. screen size #6) and stored at ~50-55 ℃ overnight to remove moisture before injection molding. Pellets were injection molded (Electro-Matic Inc, Farmington Hills, MI) at 190 ℃ into specimens for ASTM D-790[23] (flexure) and D-7205[24] (tensile) standard specimens. For the lower level PLA-CNF compositions, only tensile standard test specimens were made. For PLA-CNF films (0.1-10wt.%CNF at 20wt.% initial mix solids), the dewatered cake of material was transported directly to the oven and dried at 50 ℃ for 16 hours. A mold was prepared by folding an aluminum foil sheet multiple times until a

thickness of 0.7mm was achieved. A 50 x 50 $mm^2$ square was cut out of the sheet to provide the shape of the final films. The mold was placed on top of a Teflon-coated caul sheet, a 2 g piece of a sample cake was placed in the mold, and another Teflon-coated caul sheet was placed on top. The assembly was placed in a Carver Press (Wabash, IN) at 185 ℃, and the distance between press platens was closed until the top press platen was barely touching the top caul platen. The assembly sat for 2 minutes to allow the specimen to soften so that the Teflon layer would not be damaged during pressing. The assembly was then pressed at 155PSI/1.07MPa for 20 seconds, after which the press was opened and the assembly removed. A cold press weight (~3kg) was placed on top of the assembly to prevent the films from warping as they cooled. The films were then cut into 50 x 5 $mm^2$ rectangular strips using a Muse 3D Autofocus Desktop $CO_2$ laser cutter (Full Spectrum Laser, Las Vegas, NV).

For mechanical testing, specimens were conditioned at ~25 °C and ~50% relative humidity for at least 48 hours prior to testing. At least N=5 specimens per sample type were tested with 3 point-bending (500N load cell, crosshead speed = 1.82 mm/min) and tensile (100kN load cell, test rate = 5 mm/min) apparatus in an Instron model #5942 and Instron model #5966 universal test machine (Instron, Norwood, MA), respectively. Tensile strengths were reported in terms of ultimate tensile strength, or the highest tensile strength observed during testing. Intact portions of broken specimens from flexural testing were cut to size and notched according to ASTM D-256[25] for impact testing, conditioned as above, then tested with N=5 specimens per sample in a CEAST pendulum impact testing apparatus (Instron, Norwood, MA) with a 50 N hammer. For film testing, the laser cut strips were conditioned at ~25 °C and ~50% relative humidity for at least 48 hours, then tested for tensile strength in an Instron model #5942. The crosshead speed was 1 mm/min, and the gauge length was 35 mm. This is similar to the standardized test method used for tensile properties of thin plastic sheeting (ASTM D882)[39], except the gauge length used was far below the standard recommendation of 100-250mm for determination of tensile modulus. The laser cutting method also differs from any cutting methods recommended by the standard for cutting film and sheeting tensile test specimens (ASTM D6287)[40]. Since no uniform standards exist for testing of brittle nanocomposite films, this method was only used as a "first pass" to estimate how dewatered CNF loading

affected tensile strength before scaling up to larger-scale shear-mixed specimens. Because of the small size of the test specimens, an extensometer could not be used for accurate measurement of strain, therefore only ultimate tensile strength was reported. Multivariate ANOVA (analysis of variance) was performed to determine statistical differences in all properties tested between composite types, assuming a 95% confidence level. Waller-Duncan Post-hoc analysis was used to compare significantly different subgroups of samples.

### 3.3.3. CNF Monolayer Calculations

Theoretical calculations were performed to model the minimum amount of CNFs that can be added to a mixture with PLA particles and form a monolayer of desired thickness covering each individual particle. The purpose of this model was to understand how a system of dewatered PLA-CNF can be optimized to produce dry CNFs, as dewatering below the threshold for the monolayer formation may optimize the trapping of individual CNFs between PLA particles to produce well-dispersed, dry fibers with nanoscale dimensions. First, the surface area of a PLA particle with an assumed diameter of 1 μm was calculated assuming the particles as spheres (Equation 3):

$$A = 4\pi r^2 \quad (3)$$

where A is the surface area of a sphere, , and r is the radius of the circle. The volume of the individual PLA particles was also calculated (Equation 4):

$$V = \frac{4}{3}\pi r^3 \quad (4)$$

where V is the volume of a sphere, and r represents the same parameter as in Equation 3. Since the majority of PLA particles were under 150 μm in diameter, 1 μm was used as the starting diameter for constructing the model. The density of PLA was assumed to be 1.24 g/cm$^3$ based on the specification sheet received from the manufacturer for the PLA pellets used in this work. This density was multiplied by the calculated volume to obtain the mass per PLA particle in grams, which was then inverted to find the number of particles in a gram of PLA. CNF film density was assumed to be 1.2 g/cm$^3$, and multiplied by the theoretical volume of a CNF monolayer of a given of PLA thickness (thickness of CNF monolayer

multiplied by surface area of a PLA particle) covering the PLA particle to obtain the mass of a CNF monolayer per particle. This was multiplied by the amount of particles per gram for the assumed PLA particle diameter to obtain the total grams of monolayer-forming CNFs in a gram of PLA, which was multiplied by 100 to obtain the wt.% of CNFs in a PLA-CNF mixture required to form a monolayer of the assumed thickness. This process was performed for multiple assumed PLA particle diameters (1-100 μm) and CNF monolayer thicknesses (100, 200, 400 nm).

### 3.3.4. Polarized Light Microscopy

To observe CNF morphology within the compounded samples, thin films were pressed for polarized light microscopy (PLM) analysis. 200 mg pieces were cut from broken tensile specimens for each formulation. The pieces were placed in between Teflon-covered caul plates, then placed in a Carver Press at 185 ℃. The distance between press plates was reduced until the top press platen was barely touching the top caul plate, and the assembly sat for 2 minutes to allow the specimen to soften so that the Teflon layer would not be damaged during pressing. The assembly was then pressed at 361PSI/2.5MPa for 20 seconds, after which the press was opened and the assembly removed. A cold press weight (~3kg) was placed on top of the assembly to prevent the films from warping as they cooled. The films were placed on top of the light source of a HaYear computer microscope (Shenzhen, China) with at 0.5x magnification. A 7.6 mm piece of coir fiber was measured and cut with calipers and used as a scale bar for fibril dimension estimation. The sample was observed between cross polarizers with an additional full wave (red) filter causing the semi-crystalline, oriented CNF to exhibit birefringent colors with respect to the non-oriented, highly amorphous PLA film[41]. To obtain higher magnification images of fibrils within films, a different microscope (Amscope model ME520TA-9M, Irvine, CA) was used. For the Amscope, films were placed on top of a glass slide, and a similar polarizing setup was used. Pictures were taken with 10x objective lens, using the Amscope software to set scale bars at 50 μm. Three images per sample type were taken. A maximum magnification lens of 10x was used to ensure many particles could be measured, as the next step up (20x magnification lens) only allowed for the measurement of 3-5 particles at a time.

### 3.3.5. ImageJ Analysis

ImageJ analysis[22] was used in conjunction with PLM images to estimate particle size distributions of the shear-mixed PLA-CNF films (0.5-2wt.%, both dewatered CNF and SDCNF). The Amscope images were first imported into ImageJ, then the measurement scale was set using the on-screen 50 µm scale bar from the Amscope software. An 8 x 8 $mm^2$ square was cropped out of each image, and the channels were split into R/G/B color channels. Choosing the green color channel filtered out the magenta from the PLM images, allowing the green-yellow-blue birefringent CNFs to be more easily visualized. The images were converted into a binary black/white color scheme, and the binary color threshold was set to 54. This process is shown in Figure 13.

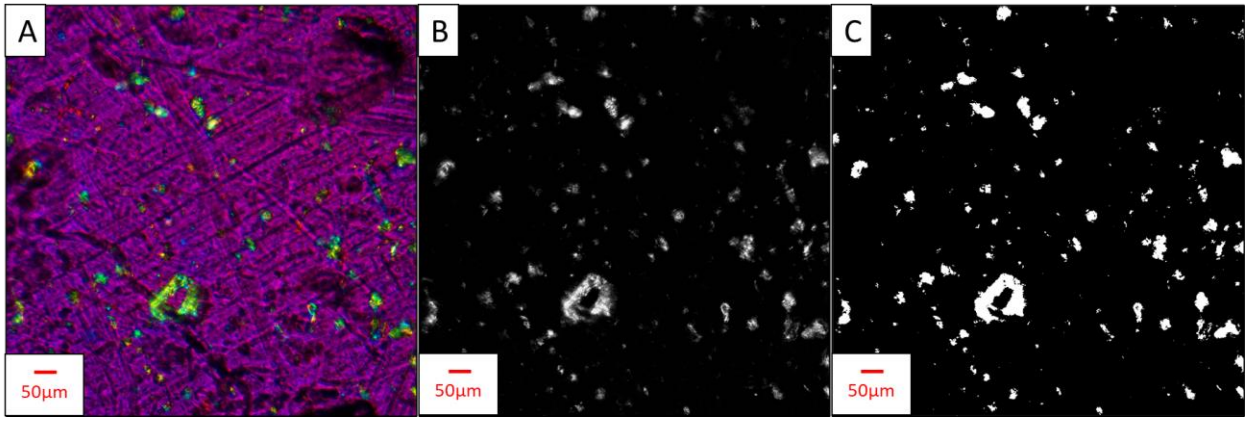


Figure 13: PLM Image processing for particle analysis of CNF in PLA-CNF films. (A): Image of PLA-0.5%SDCNF, cropped to 8 x 8 $mm^2$ with scale bar removed. (B): "Green" channel from R/G/B channel split. (C): Final binary image used in particle size analysis. Scale bar size = 50µm

The particles were analyzed using an elliptical fit model to estimate major axis ("length") and minor axis ("width") of CNF fibers in the composite. The elliptical fit model was applied by checking "area" and "fit ellipse" options under "set measurements" in the "analyze" toolbar, then analyzing particles from 0-infinity $\mu m^2$. This was done for three PLM images per sample type. The resulting data was copied into excel, and data from all three images were combined into a single dataset for each sample type. Aspect ratios were calculated by dividing the major axis by the minor axis for each particle analyzed. All datasets were randomized and scrubbed so that each contained exactly 1982 data points to

ensure equal population sizes for each dataset. Averages and histograms of major axes and aspect ratios were obtained using Sigmaplot. Normality testing was performed in SPSS using Shapiro-Wilk and Kolmogorov-Smirnov analyses. Aspect ratios were measured due to being predictors of composite performance based on percolation theory, in which fibers in a composite matrix are theorized to transition to an "infinite" communicating state upon reaching a given percolation threshold[42] (Equation 5):

$$V_{Rc} = \frac{0.7}{L/d} \qquad (5)$$

where $V_{RC}$ is the volume fraction of fibers at which they will form this communicating state and L/d is length over diameter, or aspect ratio of the fibers in the composite matrix. Higher aspect ratio fibers decrease the volume fraction of fibers needed to achieve percolation. This communication is theorized to increase mechanical properties of the final composite.

### 3.3.6. Water Removal and Energy Analysis

Three separate 100 g samples of wet mixtures from each formulation were weighed out, and moisture content was determined for each formulation to establish the starting mass of solids in the samples. Each sample was pressed at least five times using the same parameters as in the initial material manufacture section, and the mass of the remaining material was recorded after each subsequent pressing event. Paper towels under the mesh screens were replaced after each pressing event to facilitate moisture removal. The resulting solids after pressing were calculated by comparing the mass recovered to the starting solids of the material. The drying energy requirement per gram of dried CNF for each mixture was determined using a theoretical energy calculation based on the specific heat capacity of water (Equation 1), using the mass of water remaining after one press event. These results were compared to empirical data for the energy required to produce SDNCF obtained from Oak Ridge National Laboratories. The energy calculations were based on the drying and water removal process, and therefore energy considerations for cryocrushing PLA to produce powder were not included.

Hard to remove water (HRW) analysis was done in accordance with previous methods[16][26][27], and with section 2.3.3 of this thesis work. Hard to remove water content (%/%) was calculated by measuring

the total mass percent at the start of the time-dependent second derivative drop in mass, subtracting the final mass percent after drying had completed (percent solids of material), then dividing by the final mass percent (Equation 2). This was done for two samples of PLA-CNF at 10, 30, and 50wt.%CNF, with the results being reported in terms of averages of the two HRW results.

## 3.4. Results and Discussion

### 3.4.1. Material Manufacture and Characterization

Sieve analysis showed that most PLA particles received (95.6 wt.%) were below 250 μm in diameter, with particles below 150 μm making up 56 wt.% of the PLA powder. This percentage was decreased with each successive 10 wt.% CNF addition, as shown in Table 3. At 10 wt.% CNF addition, the percent of particles above 250 μm in diameter remarkably increases from 4.5% in pure PLA powder to 42.7%, and then 85.7% in PLA-50wt.%CNF. An inverse trend was observed in the smaller particle fractions, indicating that CNF is attaching to PLA particles during the drying process and increasing particle diameters.

Table 3: Sieve analysis of PLA particles and PLA-CNF mixtures

| Mixture | Fraction Diameter (μm) | Mass % |
|---|---|---|
| PLA | >250 | 4.5 |
| | 150-250 | 39.2 |
| | <150 | 56.3 |
| PLA-10%CNF | >250 | 42.7 |
| | 150-250 | 36.8 |
| | <150 | 20.5 |
| PLA-50%CNF | >250 | 85.7 |
| | 150-250 | 8.7 |
| | <150 | 5.6 |

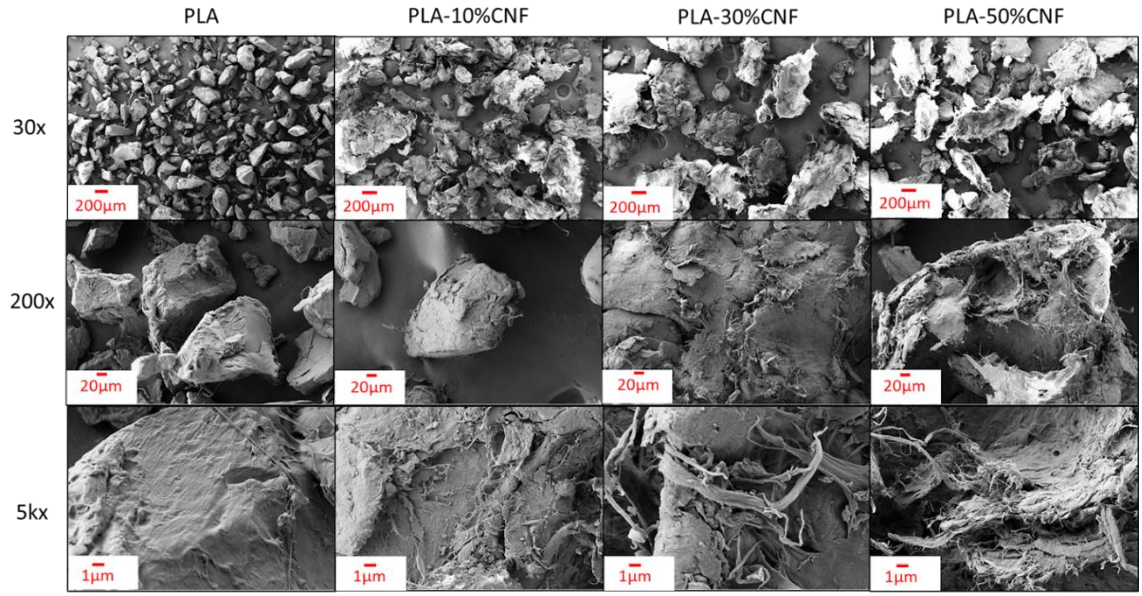


Figure 14: SEM images of dried, milled PLA-CNF mixtures.

SEM images of PLA-CNF (Figure 14) show that CNF can attach to PLA particle surfaces, and tend to agglomerate around individual PLA particles at 10-50 wt.% loading levels when mixed in a 5 wt.% solids PLA-CNF mixture. While individual nanoscale fibrils can be observed, the agglomerated form of CNF appears to dominate the overall morphology. The individual fibrils observed are more likely due to breaking up of agglomerates from grinding the dry mixtures. Smaller agglomerates are seen in PLA-10%CNF particles, with some appearing to just barely cover PLA particles. Some agglomerates appear to be almost half a millimeter in diameter, potentially adhering together multiple PLA particles. Since larger-scale CNF agglomerates appear in all mixtures from 10-50wt.% CNF, and smaller fibrils were observed after grinding, it was decided to compound while masterbatching at 50wt.%CNF. This was to examine if shear mixing could break up these larger particles to provide a better CNF morphology in the final composite.

### 3.4.2. Composite Processing and Testing

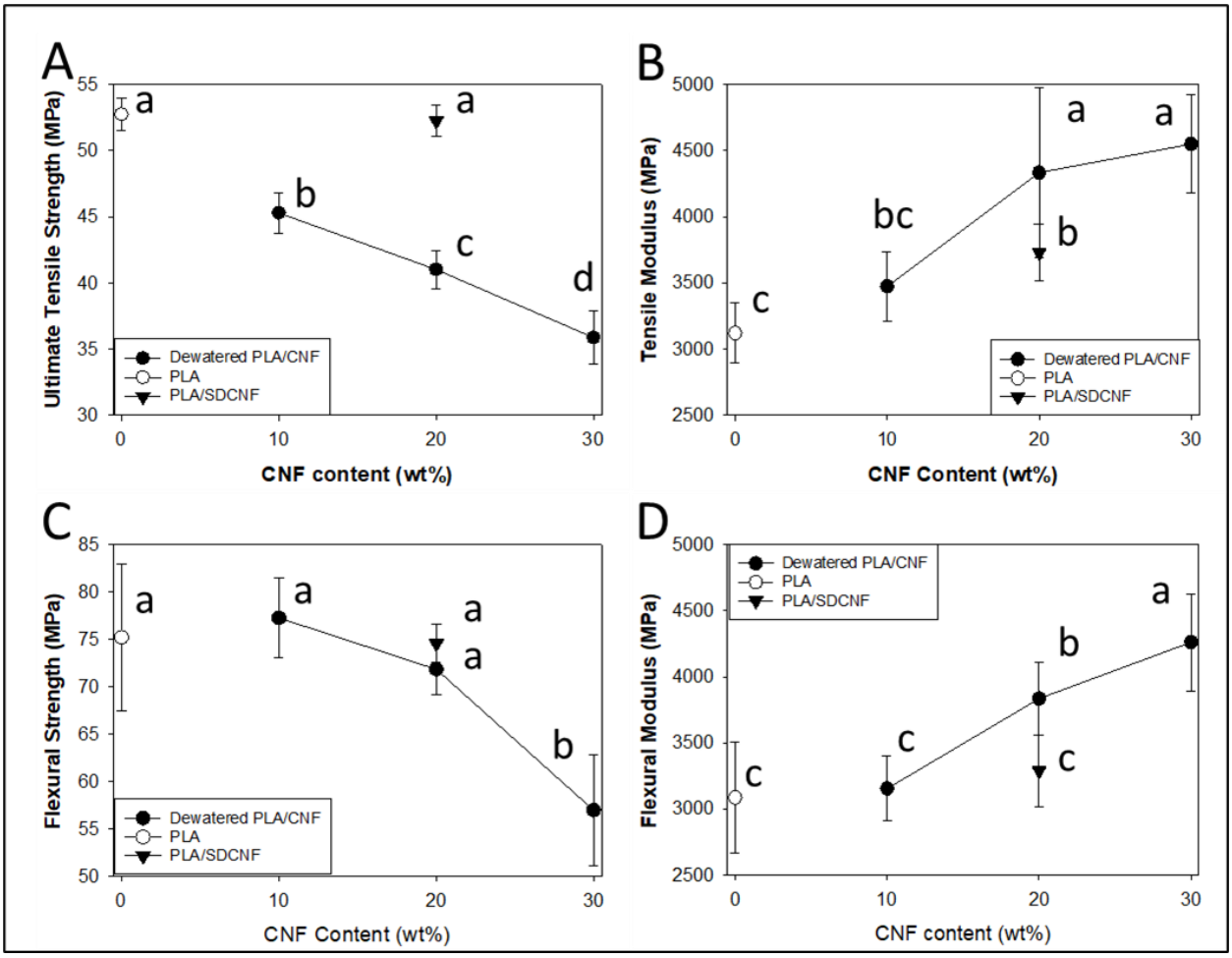


Figure 15: Tensile and Flexural testing results from masterbatched PLA-CNF composites, compared with PLA and PLA/SDCNF results from Chapter 2. (A) Tensile strength, (B) Tensile modulus, (C) Flexural Strength, and (D) Flexural Modulus. Common letters on data points indicate statistically insignificant differences at 95% confidence level.

Figure 15 shows results from initial testing of masterbatched (using PLA-50%CNF) PLA-CNF composites. The incorporation of masterbatched PLA-CNF significantly decreased the tensile strength of the final composite at 10-30wt.%CNF loading levels compared to PLA and PLA-SDCNF results from Chapter 2. The poor tensile performance is likely attributable to the sphericity and heterogeneous dispersion of the masterbatched dewatered CNF, as seen in Figure 14. Tensile modulus significantly increased compared to PLA and PLA/SDCNF at 20wt.% masterbatched CNF addition and above, indicating that the PLA is being reinforced by stiffer dewatered CNF particles, which may have had

higher aspect ratios than spherical SDCNF. Curiously, flexural strength of the composites only significantly decreased at 30wt.% masterbatched CNF addition, while 10-20wt.%CNF showed similar flexural strength to the two controls. Flexural modulus increased similarly to tensile modulus, with each 10wt.%CNF loading level significantly increasing flexural modulus. No significant difference in impact strength was observed between PLA, PLA-20%SDCNF, and the masterbatched PLA-CNF mixtures until 30wt.% masterbatched PLA-CNF, where the impact strength significantly decreased to 19 J/m (28 J/m for PLA) (Table 5). Since impact testing specimens were made from broken flexural test specimens, residual stresses may have reduced overall material toughness. Despite this, the difference in impact strength between sample groups shows that CNF addition to composites influences likely impact strength.

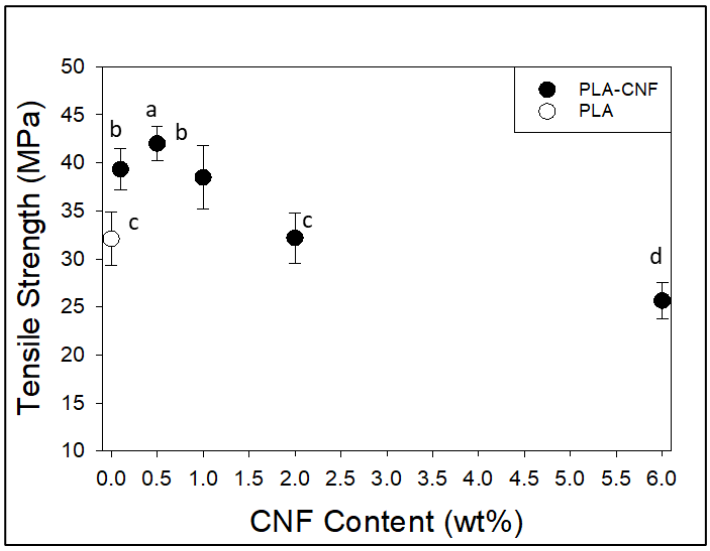


Figure 16: Tensile Strength of compression molded PLA-CNF films as a function of CNF content.

Film testing results (Figure 16) show that dewatered CNF loading into hot pressed films significantly increases film tensile strength compared to pure PLA at 0.1-1wt.%CNF loading levels, with a reduction in tensile strength above 2wt.%CNF. The tensile strength of PLA here (32MPa) is much lower than those observed from ASTM samples (~54MPa). This may be attributable to the laser cutting method to prepare the tensile testing strips, which used a pulsed laser that may have created serrated edges with defect points that weakened the test specimens compared to the smoother surface of injection molded specimens. If the press time or pressure was not enough to homogenize properties of thin films

from powder PLA, then hot pressing parameters may have also contributed to a weaker thin film strength. A similar result was seen in another work utilizing chitin nanocrystals in a thin film PLA composite, where the control PLA film showed an ultimate tensile strength of 44MPa[43]. The cutting method for this work was not specified. This does not provide a strong comparison to how injection molded specimens will perform in tensile testing but can act as a "first pass" method to determine how CNF incorporation is affecting the tensile properties of PLA. Despite this comparative weakness in PLA, coefficients of variation were low across all sample types (2-9%), indicating that the differences seen between different films can be attributed mostly to CNF loading level.

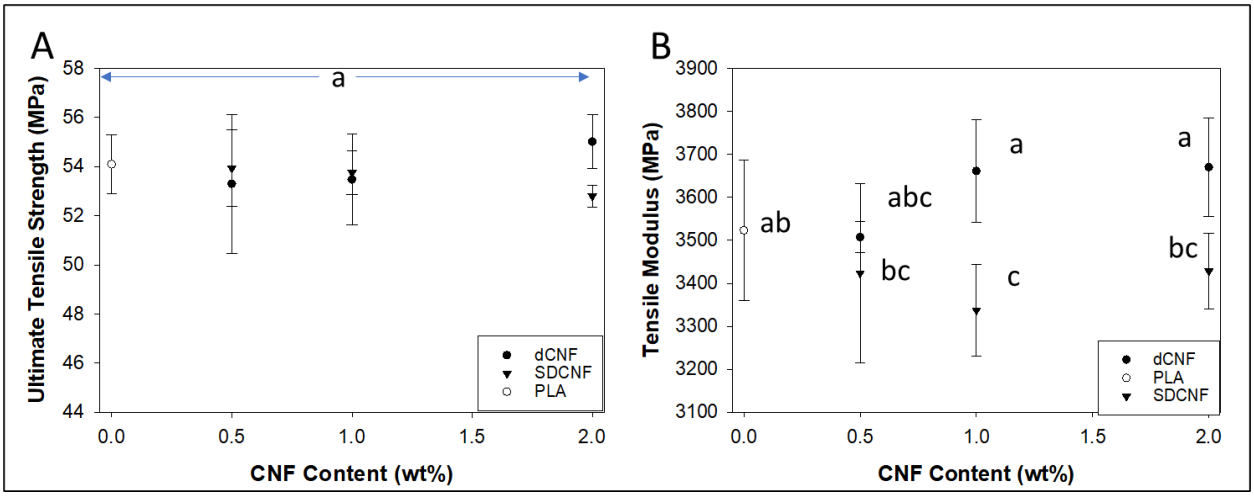


Figure 17: Ultimate tensile strength (A) and tensile modulus (B) of shear-mixed dewatered PLA-CNF composites at 0.5-2wt.% loading.

In shear-mixed composites (Figure 17), dewatered CNF (dCNF) does not significantly increase tensile strength or modulus compared to pure PLA up to 2wt.%dCNF, although a 1.7% increase in average ultimate tensile strength and a 4.2% increase in average tensile modulus compared to PLA was observed. dCNF composites had similar or better ultimate tensile strength and tensile modulus values than SDCNF composites at the same CNF loading levels.

### 3.4.3. CNF Monolayer Calculations

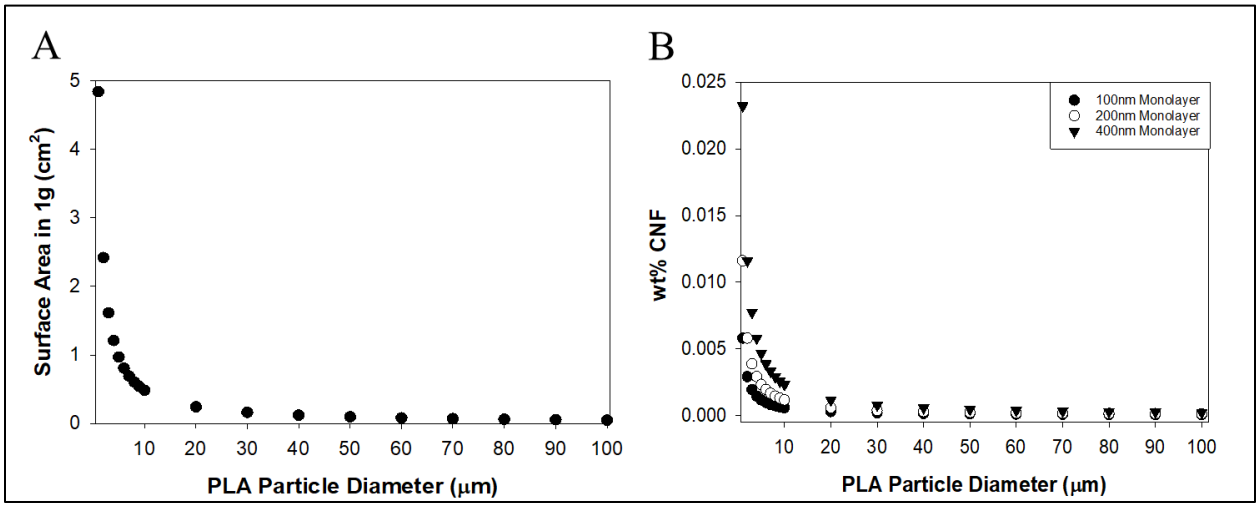


Figure 18: (A) Total estimated surface area in 1g PLA particles over particle diameter. (B) Estimated threshold wt.% CNFs in PLA required to form a monolayer over each PLA particle based on PLA particle diameter.

Based on the monolayer formation model developed in Section 3.3.3, a 400 nm – thick monolayer of CNFs should form over each individual PLA particle in a PLA-CNF mixture at 0.023 wt.% CNFs assuming a PLA particle diameter of 1 μm (Figure 18B). This value drops to 0.012 and 0.005 wt.% CNFs for 200 and 100 nm monolayers, respectively. Below these values, it can be assumed that CNFs remain well-dispersed as fibrils without forming agglomerates around individual PLA particles as seen in the SEM results from section 3.4.1. The wt.% values for monolayer formation decreased in a power relationship ($R^2$=1) based on particle diameter, like the relationship between overall surface area of 1g of PLA particles and particle diameter (Figure 18A). This shows that available surface area is likely the major factor behind whether CNFs form agglomerates or monolayers around PLA particles. At PLA particle diameters of 20 μm and above, the model begins to asymptote toward zero, indicating vanishingly small amounts of CNF causing agglomeration around PLA particles. This model does not account for dispersion of CNFs in PLA at varying total mixture weight percents and can be made more accurate through empirical observation of the PLA-CNF agglomeration process. The model also assumes uniform particle diameters, while the actual particles had highly variable diameters (Table 3). Despite the

limitations of this model, the low wt.%CNF agglomeration thresholds observed here helped to inform the decision to lower dCNF loading into PLA to 2wt.% and below.

### 3.4.4. Polarized Light Microscopy

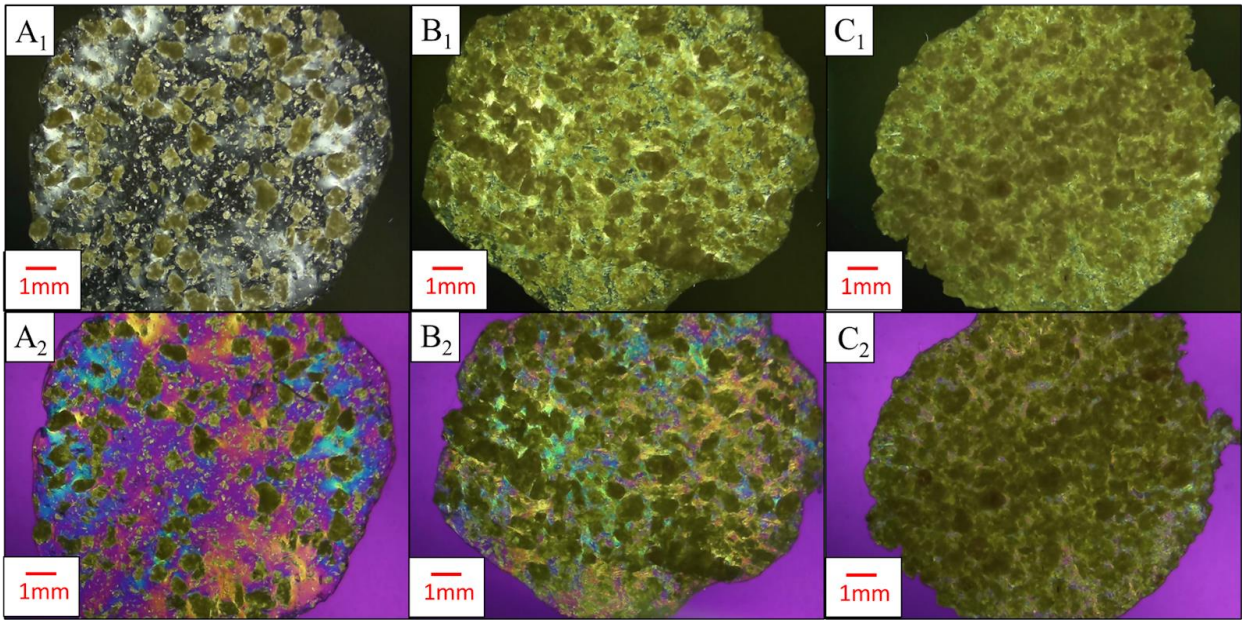


Figure 19: Polarized light microscopy images of PLA-CNF composites made from masterbatched PLA-50%CNF. Letters correspond to CNF loading level, numbers correspond to microscopy type . A, B, C: 10, 20, 30wt.%CNF. 1, 2: PLM between crossed polarizers without a retardation filter, PLM between crossed polarizers with a retardation filter. Magnification: 0.5x

Results from polarized light microscopy of masterbatched PLA-CNF films are shown in Figure 19. CNF particles exhibit birefringent blue/yellow/green colors, while the non-birefringent PLA background is purple/magenta. Thicker agglomerates of CNF do not let the light pass and are visually dark green or yellow. In the 10wt.%CNF cross-polarized image (Figure 19$A_2$), blue-yellow film regions with no visible particles were observed in the PLA film, which correspond to white regions observed in the film with only one polarizing filter (Figure 19$A_1$). This may be attributed to CNF increasing the crystallinity of the polymer film, therefore providing crystalline orientation that can be observed with PLM, although this has not been confirmed by more accurate methods for determining crystallinity such as Differential Scanning Calorimetry (DSC). The morphology of CNF in the films is dominated by spherical agglomerates up to a

millimeter in diameter. Smaller and higher aspect ratio particles are observed in the PLA-10%CNF film (Figure 15$A_2$), and colored domains where no visible fibers can be observed exist in the film. As CNF loading is increased, the dispersion of the CNF agglomerates is reduced, and particles contact each other more frequently within the PLA. This "crowding" effect could have caused the increased moduli and decreased strength of the composites seen in Figure 15. The moduli increased attributable to the higher stiffness of interacting CNF particles in the PLA composite, but the mechanical strength decreased because of poor dispersion of the crowding PLA particles and the large size and low aspect ratios preventing the percolation effect for reinforcement. These results along with the SEM images in Figure 14 showed that PLA particles did not effectively "trap" CNFs and prevent agglomeration at 10-50wt.% loading levels. This observation was instrumental in the decision to lower the CNF loading levels to determine the threshold at which CNFs would be effectively "trapped" by PLA particles during dewatering and drying.

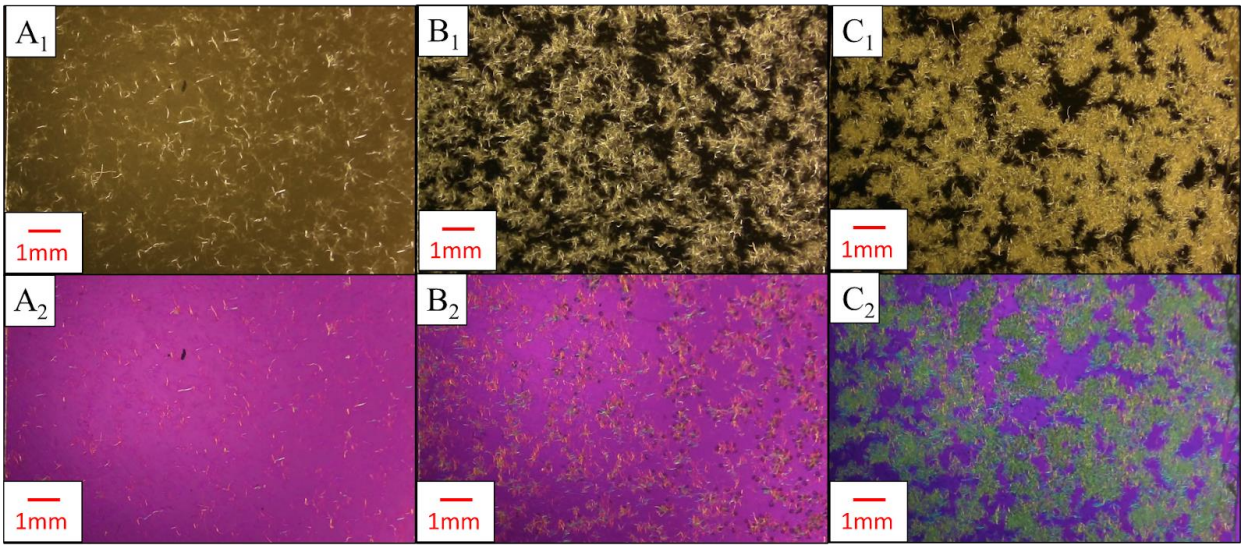


Figure 20: Polarized light microscopy images of PLA-CNF composites made at lower CNF loading levels. Letters correspond to CNF loading level, numbers correspond to microscopy type. A, B, C: 0.5, 2, 6 wt.%CNF. 1, 2: PLM between crossed polarizers without a retardation filter, PLM between crossed polarizers with a retardation filter. Magnification: 0.5x.

Figure 20 shows that reducing CNF loading levels in the dewatered mixtures better preserves fibril dimensions after drying. Fibrils appear well-dispersed in the 0.5 wt.%CNF film, with fibrils forming

lightly agglomerated networks at 2 wt.%CNF. This is likely around the threshold at which the PLA particles are capable of trapping and dispersing CNF particles to prevent agglomeration, shown by the reduction of film mechanical properties at 2 wt.%CNF in Figure 16. This agglomeration increases with higher CNF loading, shown by the heterogeneously dispersed millimeter-scale structures CNF observed in 6 wt.%CNF films (Figure 16$C_2$), along with the further decrease in film tensile strength at this loading level.

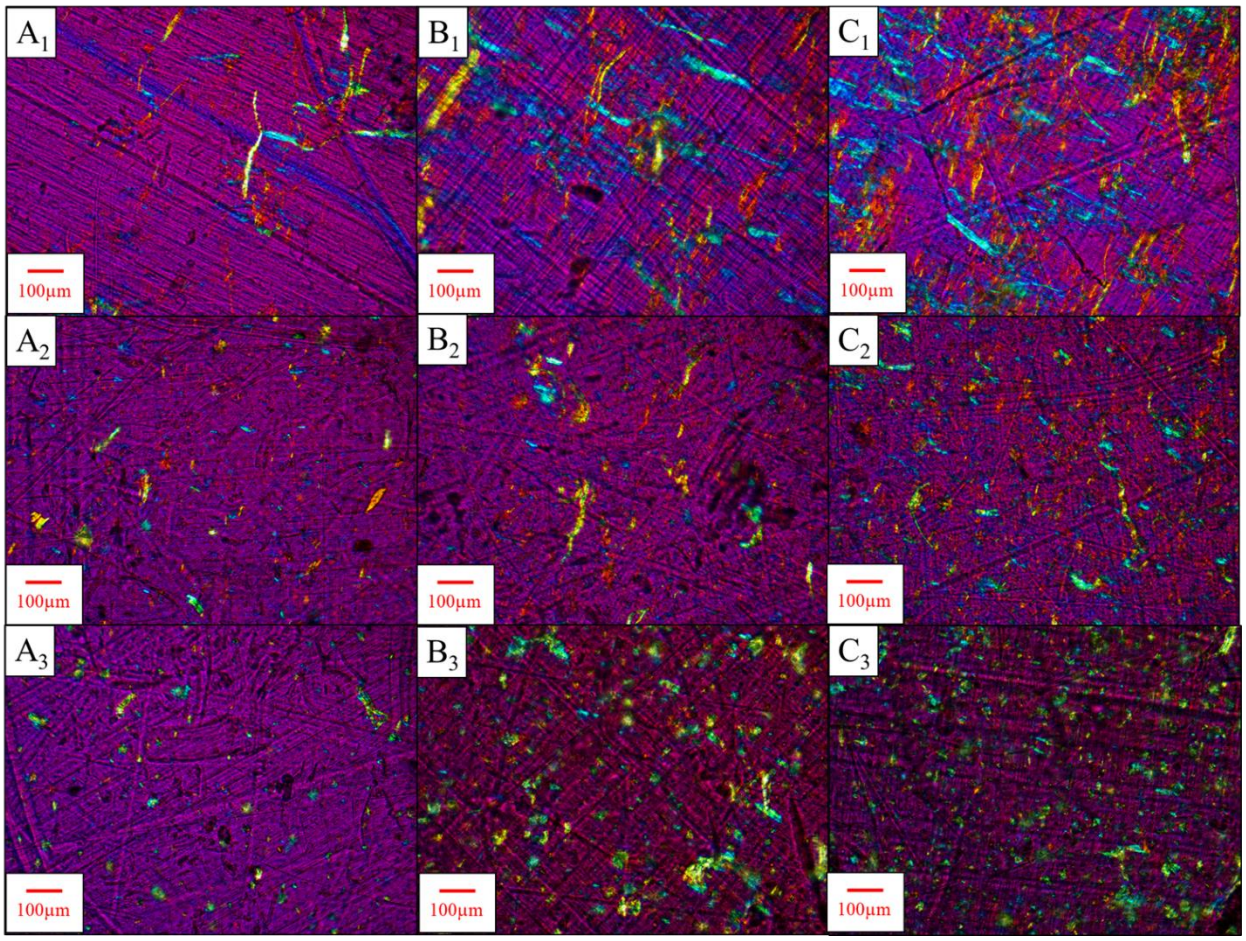


Figure 21: PLM images of PLA-CNF films at lower loading levels of CNF. Letters correspond to CNF loading level, numbers correspond to processing/CNF type. A, B, C: 0.5, 1, 2wt.%CNF. 1, 2, 3: compression molded PLA-dCNF films, shear mixed PLA-dCNF, shear mixed PLA-SDCNF. Objective lens: 10x.

In Figure 21, reddish fibril networks can be observed in the non-compounded dewatered PLA-2%dCNF film (Figure 21$C_1$), which can be attributed to CNF fibrils that are out of phase with the polarized light beam passing through the sample. CNF fibers with maximum widths approaching 45 µm

for dewatered CNF and 70 μm for SDCNF were observed, with most particles appearing to be 10s of microns in width. Shear mixing reduced the overall fibril lengths, broke up loosely associated fibril networks in PLA-2 wt.% dCNF to produce dispersed CNF fibrils with similar dimensions to PLA-0.5/1 wt.%dCNF. This could explain the differences in mechanical properties between dewatered CNF-loaded samples with and without shear mixing , as the agglomerated networks in the PLA-2%dCNF film that may have reduced tensile strength were converted into loosely percolating fibrils that slightly increased the tensile strength and stiffness of the final shear-mixed composite. Since PLA-2 wt %dCNF was the maximum loading level tested here, and showed better relative properties to PLA in shear-mixed samples than in films because of this fibril breakup and dispersion during shear mixing, higher levels of CNF loading may also produce similar effects after shear mixing, but the threshold at which CNF can be dewatered and shear mixed without reducing the tensile properties of the final composite has not been determined.

The non-shear mixed films (Figure 21$A_1$-$C_1$) showed much longer fibers that were difficult to measure using ImageJ software macros, but individual fiber measurements showed that fibers were hundreds of nanometers to tens of microns in width, and typically hundreds of micrometers in length, although nanoscale dimensions are not directly observed within the resolution of optical microscopy. These yielded high aspect ratios (up to 112), which may have significantly reduced the percolation threshold for fibers in the final composite, hence why the highest tensile properties in dewatered PLA-CNF films were seen from 0.1-1 wt.%CNF loading. The highest tensile properties in shear mixed PLA-dCNF composites were seen at 2 wt.%, which may indicate overall fiber aspect ratios and therefore a higher CNF loading level required to reach percolation threshold. Overall, the dewatered CNF appears to have more fibrous and fewer spherical structures than SDCNF, which can explain the higher tensile properties at 1-2 wt.% dewatered CNF. The fibrous structures seen in PLA-0.5%dCNF films do not correspond to the earlier models of CNFs forming spherical monolayers around PLA particles at 0.025 wt.% and below, indicating that the model needs to be adjusted to properly account for how CNFs agglomerate in PLA-CNF mixtures. Since agglomeration is more clearly seen at 2wt.%dCNF and above,

where film tensile strength begins to decrease, this is likely closer to the "monolayer formation" or agglomeration threshold at 20 wt.% mixing solids.

### 3.4.5. ImageJ Analysis

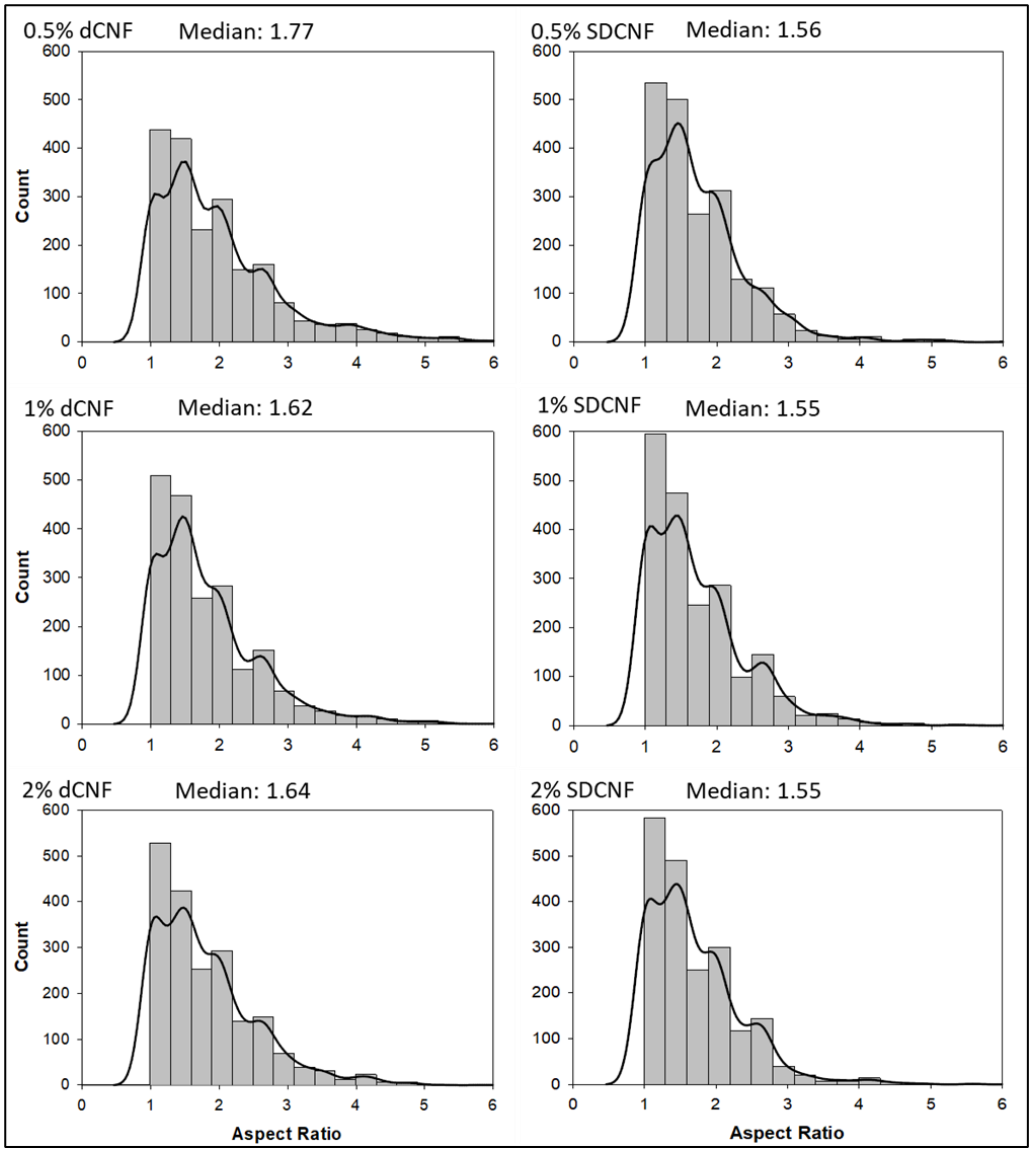


Figure 22: Aspect ratio histograms from analysis of PLA-dCNF and PLA-SDCNF PLM images. Bin size = 0.333 μm /μm. Bandwidth for kernel density overlay= $1.507*10^{-1}$. Median aspect ratios listed above each distribution.

Aspect ratio distributions from ImageJ analysis (Figure 22) show most particles measured had aspect ratios between 1 and 5. All distributions have high positive skew (>2), and most measured particles had aspect ratios below 2. All SDCNF composites showed a higher count of particles with aspect ratios

below 2, especially between 1-1.667. Shapiro-Wilk and Kolmogorov-Smirnoff tests rejected the normality of all datasets, indicating that averages, standard deviations, and standard hypothesis testing to quantify differences between datasets may be unreliable. Medians of all datasets were therefore reported, with all dewatered CNF composites showing higher median CNF aspect ratios than SDCNF composites. The higher CNF aspect ratios may have contributed to the higher mechanical properties seen with dCNF compared to SDCNF at similar loading levels (Figure 17), even if the quantified differences among datasets is small. The analysis used an elliptical fit model, which may have caused issues in accurately measuring the length of longer fibrils with variable widths and orientations. The maximum measured aspect ratio range for dCNF datasets (8.3 for PLA-2%dCNF to 16.7 for PLA-0.5%dCNF) was higher than that of SDCNF datasets (6.2 to 10.1). The minimum measured particle minor or major axes for all datasets was 0.371 μm (371 nm), which was also the mode for each dataset. This indicates that 371 nm is probably the lower limit for length measurement in this analysis method. Dry fibrils at least hundreds of nanometers in width were likely preserved after drying, and fibrils with even smaller widths may exist but not have been detected by the software. The wavelength of visible light is between 380 to 700nm, so 371nm is below the lower level of detection for this method. This may have also led to inaccuracies in final aspect ratio measurement, as fibers below 380 nm in width should not have been measured using this method. Only using the "green" color channel may have prevented the software from preventing other birefringence colors, such as blue, and therefore reduced the overall measured particle size. Even with these potential issues in measurement, this can be used as a first-pass method to indicate how aspect ratios of dewatered CNF compare to Spray-Dried CNF, as shown by the different median aspect ratios between the two groups, and the relatively similar median aspect ratios within the SDCNF measurements.

### 3.4.6. Water Removal and Energy Analysis

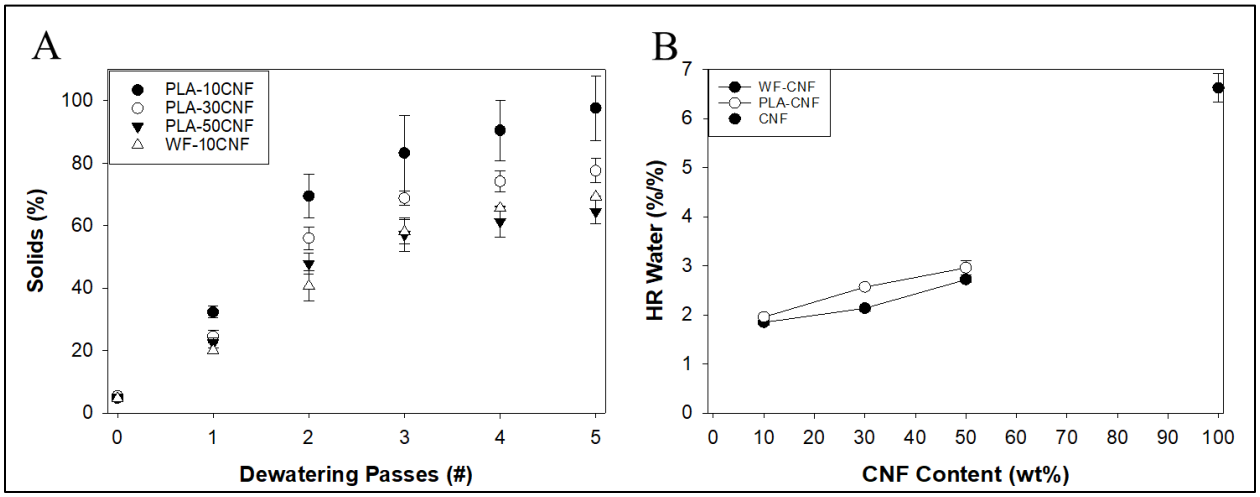


Figure 23: (A) Percent solids of PLA-CNF mixtures after multiple dewatering passes, compared to WF-10%CNF from . (B) HR water contents of PLA-CNF and WF-CNF furnishes (CNFs at ~3% solids, mixtures at ~5% solids).

As seen in Figure 23A, water removal shown by final wt.% solids was calculated based on the starting moisture content and mass of pressed furnish from 10-50 wt.%. PLA-CNF seems to follow a polynomial relationship with number of presses ($R^2$ = 0.98 - 0.99), which begins to asymptote for PLA-50%CNF at 60 wt.% solids, PLA-30%CNF at 74 wt.% solids, and PLA-10%CNF between 80-99% solids. Water removal for PLA-CNF mixtures was much higher than WF-CNF furnishes from Chapter 2 at similar loading levels, possibly due to the smaller PLA particle size, with 95.6 wt.% and 23 wt.% of PLA particles and maple WF fibers, respectively having diameters below 250 µm (Tables 3 and 4). The smaller size of PLA particles and therefore higher surface area for solid PLA to contact wet CNF fibrils likely caused more efficient dewatering. Wood flour can also hold approximately 30% of its dry weight in water (70 wt.% solids fiber saturation point), while water saturation capacity for less porous, less hydrophilic PLA is likely a lot lower. PLA-10%CNF solids had much higher standard deviations than all other mixtures. At 5 wt.% solids, the PLA-10 wt.%CNF mixture was much less viscous than all others, which may have led to material loss during pressing and therefore discrepancies in dewatering results. HR Water results (Figure 23B) show that, while water removal is higher using PLA to dewater CNF compared to WF, this does not correlate to different levels of tightly bound water between the dewatering

material types, as PLA-CNF mixtures had slightly higher HR water contents than WF-CNF furnishes at similar loading levels.

Similar properties were seen with dewatering lower levels of CNF (Figure 24A) at 20 wt.% solids, with solids content showing asymptotes around 79% for PLA-2%CNF, 86% for PLA-1%CNF, and 87% for PLA-0.5%CNF. The solids content increased more after 1 press (from 20 to ~60 wt.% solids) for all low-level CNF mixtures compared to the high-level CNF mixtures (from 5 to ~30 wt.% solids), likely due to the higher solids content facilitating water removal from the system. The solids content asymptote around 79-87% as well as the low standard deviation confirms the previous observation that this method may be able to achieve 80-90% solids for dewatered CNF mixtures. This may also correlate with the amount of water retained by PLA itself, as the increase in water removal as shown by solids content is negligible between 0.5-1 wt.% CNF.

Theoretical energy required to dry the system per gram of "dry" CNF (Figure 24B) based only on the amount of remaining water in the sample was more favorable for dewatered CNF than for empirical values obtained from the Oak Ridge National Laboratories data on spray drying process. Compared to the 3465.2 kJ/gCNF for SDCNF, PLA-2%CNF showed a theoretical drying energy of 101.3 kJ/gCNF after just one dewatering pass, or a 34-fold reduction in energy use. PLA-50%CNF showed a theoretical drying energy of 17.8 kJ/gCNF after one dewatering pass, or a 195-fold reduction in energy use compared to SDCNF, but the unfavorable mechanical properties shown from masterbatching PLA-50%CNF may negate any advantage in energy savings. PLA-2%dCNF showed a theoretical dewatering energy of 35.8 kJ/g after 5 presses. An approximately 33-fold increase in specific drying energy between lab-scale dewatering and empirical scale-up results was observed in section 2.4.4. While scale-up work for PLA-2%dCNF has not been performed, if this 33-fold increase in energy consumption is the same for scaling up dewatered PLA-2%dCNF, it can be expected that scaled-up PLA-2%dCNF will have a specific drying energy of 1180.2 kJ/gCNF, or 2.9-fold decrease (65.9%) in specific drying energy compared to SDCNF after large-scale pressing, oven drying, and grinding.

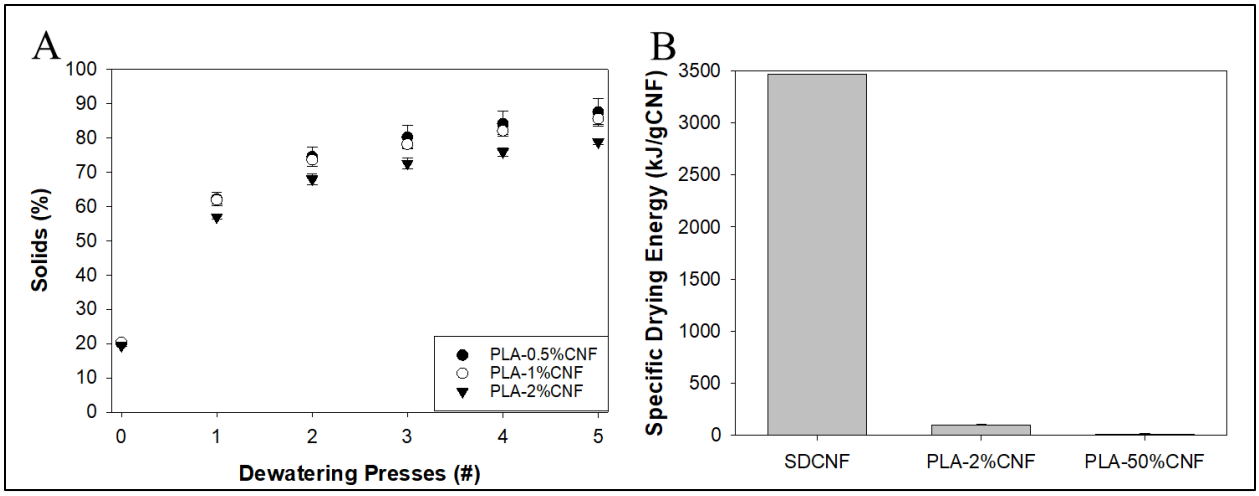


Figure 24: (A) Percent solids of low CNF mixtures after multiple dewatering passes. (B) Theoretical specific drying energy per gram of CNFs calculated for PLA-2%dCNF (20 wt.% starting solids) and PLA-50%dCNF (5 wt.% starting solids) after 1x dewatering passes compared to 1x pressed CNFs.

## 3.5. Conclusions

CNFs were successfully dewatered using PLA particles, showing promising potential for dewatering in PLA-CNF composite processing. While dewatering 10-50 wt.%CNF onto PLA was shown to be energy efficient compared to spray dried CNF, the mechanical strength of the resulting masterbatched composites at PLA-50 wt.%CNF was poor compared to pure PLA. These results were confirmed by the observation of agglomerated CNFs in SEM and PLM, showing that dewatering at these CNF levels does not produce well-dispersed, fibrillar dry CNFs ideal for composite reinforcement. By reducing the CNF loading levels, more favorable properties were achieved in hot pressed films and shear mixed composites, with a 31% increase in tensile strength compared to pure PLA by using 0.5 wt.% dCNF in films and a 1.4 and 4.2% increase in ultimate tensile strength and modulus compared to pure PLA by using 2 wt.% dCNF.

# 4. FINAL CONCLUSIONS AND FUTURE WORK

In this work, CNFs were dewatered using maple wood flour and cryocrushed poly(lactic) acid powder for the manufacture of fully bio-based polymer composites. Nanoscale CNF fibrils were observed on the surface of WF after drying, which is an improvement over many drying methods for CNFs that form agglomerated sheets, foams, or spheres. When compounded with PLA, the WF-CNF and WF-LCNF furnishes had varying effects on the mechanical properties of the final composites, as PLA/WF/CNF and PLA/WF/LCNF composites with higher CNF/LCNF content had better flexural and impact strength but worse tensile strength. The strongest composite in tensile testing was 80/18/2 (wt.% PLA/WF/CNF), which showed similar tensile strength to pure PLA, as well PLA/WF and PLA/SDCNF at 20 wt.% loading levels, as well as the highest tensile modulus of all tested composites. Energy analysis showed that up to 70 wt.% solids were achieved by simple mechanical pressing of the materials, which lowered the specific energy required to dry CNFs/LCNFs while dispersing them and reducing agglomeration. Although some water removal efficiency was lost when the process was scaled-up to produce 50lbs/22.7kg of PLA/WF/CNF composite material, the overall process required 84% less energy to produce a gram of dried CNFs than an industrially-scaled spray drying process, indicating the viability of this method for large-scale drying of CNFs. Since only 2-10 wt.% total CNF loading was tested in the composites, and the highest tensile properties were seen in the lowest wt.% CNF composite, lower levels of CNF loading onto WF should be evaluated for these composites. Scaled-up press parameters (press surface area, amount of presses, water removal from the press) should be optimized to maximize the energy efficiency of this method for drying CNFs.

Directly dewatering CNFs with PLA showed high levels of agglomeration at 10-50 wt.%CNF that reduced fibril aspect ratios and overall composite mechanical performance despite higher efficiency in dewatering than WF. When the CNF loading was reduced to lower levels (0.1-2 wt.%), nano-to-microscale CNF dimensions were observed in pressed PLA films, showing that fibril dimensions can be achieved in dewatering without the use of WF. In compression molded films, CNFs significantly increased the tensile properties of PLA from 0.1-1 wt.%, but agglomeration at 2

wt.% and above reduced tensile strength compared to pure PLA. In shear-mixed composites, PLA with dewatered CNFs showed comparable tensile strength and better tensile modulus than pure PLA or PLA with SDCNF at 1-2 wt.% dewatered CNF loading levels. Modeling the agglomeration threshold based on spherical agglomerates did not agree with results obtained from PLM image analysis, so the model assumptions should be updated to more accurately reflect the fibril agglomeration seen in 2 wt.%CNF and above. Shear-mixed PLA-dCNF composites at 0.5-2 wt.%CNFs should be tested in flexural and impact testing and compared to results for PLA-SDCNF composites at the same loading levels to provide a more thorough understanding of how dewatered CNFs affect mechanical properties at these levels. Since shear-mixing PLA-2 wt.%dCNF broke up agglomerates seen in compression molded films and produced test samples with the highest tensile properties, higher loading levels of PLA-dCNF should be shear-mixed and tested to determine the maximum level of CNFs that can be dewatered onto PLA without reducing mechanical properties. PLA crystallinity based on dewatered CNF content should be obtained to determine if the colored regions without fibers observed in Figures $19A_1$ and $19A_2$ are due to increased PLA orientation and crystallinity. If possible, smaller sizes of PLA particles and different mix solids should be tested for their ability to aid CNF dispersion and prevent agglomeration. Dewatered CNFs should be removed from PLA particle mixtures via selective dissolution of PLA or other methods to confirm dry CNF fiber size and morphology via other methods than PLM. The ImageJ analysis method with PLM should be updated to filter out data points below 380 nm in length, as visible light cannot be measured underneath that wavelength. The PLA-CNF dewatering process should be scaled up and tested similarly to the WF-CNF scale-up process in order to determine if theoretical energy efficiency compared to SDCNF remains, and the energy required to cryocrush PLA into fine powder should be considered in this analysis.

## BIBLIOGRAPHY


1. Derraik, J. G. (2002). The pollution of the marine environment by plastic debris: a review. *Marine pollution bulletin*, *44*(9), 842-852.

2. Cole, M., Lindeque, P., Halsband, C., & Galloway, T. S. (2011). Microplastics as contaminants in the marine environment: a review. *Marine pollution bulletin*, *62*(12), 2588-2597.

3. Sorrell, S., Speirs, J., Bentley, R., Brandt, A., & Miller, R. (2010). Global oil depletion: A review of the evidence. *Energy Policy*, *38*(9), 5290-5295..

4. Ke, T., & Sun, X. (2001). Effects of moisture content and heat treatment on the physical properties of starch and poly (lactic acid) blends. *Journal of Applied Polymer Science*, *81*(12), 3069-3082.

5. Klemm, D., Heublein, B., Fink, H. P., & Bohn, A. (2005). Cellulose: fascinating biopolymer and sustainable raw material. *Angewandte chemie international edition*, *44*(22), 3358-3393.

6. Zhai, L., Kim, H. C., Kim, J. W., Kang, J., & Kim, J. (2018). Elastic moduli of cellulose nanofibers isolated from various cellulose resources by using aqueous counter collision. *Cellulose*, *25*(7), 4261-4268.

7. Moon, R. J., Martini, A., Nairn, J., Simonsen, J., & Youngblood, J. (2011). Cellulose nanomaterials review: structure, properties and nanocomposites. *Chemical Society Reviews*, *40*(7), 3941-3994.

8. Pérez, J., Munoz-Dorado, J., De la Rubia, T. D. L. R., & Martinez, J. (2002). Biodegradation and biological treatments of cellulose, hemicellulose and lignin: an overview. *International microbiology*, *5*(2), 53-63.

9. Moon, D., Sagisaka, M., Tahara, K., & Tsukahara, K. (2017). Progress towards sustainable production: environmental, economic, and social assessments of the cellulose nanofiber production process. *Sustainability*, *9*(12), 2368.

10. Listo, Ariel, "Past, Present and Future of Maine's Pulp and Paper Industry." Electronic Theses and Dissertations, 2018. https://digitalcommons.library.umaine.edu/etd/2903

11. Peng Y, Gardner DJ, Han Y. Drying cellulose nanofibrils: In search of a suitable method. Cellulose 2011; 19: 91–102. doi:10.1007/s10570-011-9630-z.

12. Fu, S. Y., Feng, X. Q., Lauke, B., & Mai, Y. W. (2008). Effects of particle size, particle/matrix interface adhesion and particle loading on mechanical properties of particulate–polymer composites. *Composites Part B: Engineering*, *39*(6), 933-961.

13. Wilson, J. M., McKinney, L. J., Theerarattananoon, K., Ballard, T. C., Wang, D., Staggenborg, S. A., & Vadlani, P. V. (2014). Energy and cost for pelleting and transportation of select cellulosic biomass feedstocks for ethanol production. *Applied Engineering in Agriculture*, *30*(1), 77-85.

14. Baker, C. G. J., & McKenzie, K. A. (2005). Energy consumption of industrial spray dryers. *Drying Technology*, *23*(1-2), 365-386.

15. Tajvidi, M., Gardner, D. J., & Bousfield, D. W. (2016). Cellulose nanomaterials as binders: laminate and particulate systems. *Journal of Renewable Materials*, *4*(5), 365-376.

16. Amini, E. N., Tajvidi, M., Bousfield, D. W., Gardner, D. J., & Shaler, S. M. (2019). Dewatering behavior of a wood-cellulose nanofibril particulate system. *Scientific Reports*, *9*(1), 1-10.

17. Diop, C. I. K., Tajvidi, M., Bilodeau, M. A., Bousfield, D. W., & Hunt, J. F. (2017). Evaluation of the incorporation of lignocellulose nanofibrils as sustainable adhesive replacement in medium density fiberboards. *Industrial crops and products*, *109*, 27-36.

18. Chen, Y., Fan, D., Han, Y., Lyu, S., Lu, Y., Li, G., ... & Wang, S. (2018). Effect of high residual lignin on the properties of cellulose nanofibrils/films. *Cellulose*, *25*(11), 6421-6431.

19. Sahoo, S., Misra, M., & Mohanty, A. K. (2013). Effect of compatibilizer and fillers on the properties of injection molded lignin-based hybrid green composites. *Journal of Applied Polymer Science*, *127*(5), 4110-4121.

20. Murayama, K., Yamamoto, M., Kobori, H., Kojima, Y., Suzuki, S., Aoki, K., ... & Okamoto, M. (2018). Mechanical and physical properties of wood–plastic composites containing cellulose nanofibers added to wood flour. *Forest products journal*, *68*(4), 398-404.

21. Li, J., Li, D., Song, Z., Shang, S., & Guo, Y. (2016). Preparation and properties of wood plastic composite reinforced by ultralong cellulose nanofibers. *Polymer Composites*, *37*(4), 1206-1215.

22. Schneider, C. A., Rasband, W. S., & Eliceiri, K. W. (2012). NIH Image to ImageJ: 25 years of image analysis. *Nature methods*, *9*(7), 671-675.

23. ASTM D790-17, Standard Test Methods for Flexural Properties of Unreinforced and Reinforced Plastics and Electrical Insulating Materials, ASTM International, West Conshohocken, PA, 2017, www.astm.org

24. ASTM D7205 / D7205M-06(2016), Standard Test Method for Tensile Properties of Fiber Reinforced Polymer Matrix Composite Bars, ASTM International, West Conshohocken, PA, 2016, www.astm.org

25. ASTM D256-10(2018), Standard Test Methods for Determining the Izod Pendulum Impact Resistance of Plastics, ASTM International, West Conshohocken, PA, 2018, www.astm.org

26. Park, S., Venditti, R. A., Jameel, H., & Pawlak, J. J. (2006). Hard to remove water in cellulose fibers characterized by high resolution thermogravimetric analysis-methods development. *Cellulose*, *13*(1), 23-30.

27. Hatakeyama, T., Nakamura, K., & Hatakeyama, H. (2000). Vaporization of bound water associated with cellulose fibres. *Thermochimica acta*, *352*, 233-239.

28. Amini, E., Hafez, I., Tajvidi, M., & Bousfield, D. W. (2020). Cellulose and lignocellulose nanofibril suspensions and films: a comparison. *Carbohydrate Polymers*, *250*, 117011.

29. Joy, D. C., & Joy, C. S. (1996). Low voltage scanning electron microscopy. *Micron*, *27*(3-4), 247-263.

30. Nagardeolekar, A., Ovadias, M., Dongre, P., & Bujanovic, B. (2021). Prospects and challenges of using lignin for thermoplastic materials. *Lignin Utilization Strategies: From Processing to Applications*, 231-271.

31. Shofner, M. L., Lozano, K., Rodríguez-Macías, F. J., & Barrera, E. V. (2003). Nanofiber-reinforced polymers prepared by fused deposition modeling. *Journal of applied polymer science*, *89*(11), 3081-3090.

32. Wang, Lu, "Spray-Dried Cellulose Nanofibril-Reinforced Polypropylene Composites for Extrusion-Based Additive Manufacturing." Electronic Theses and Dissertations, 2017. https://digitalcommons.library.umaine.edu/etd/2791/

33. Moberg, T., Sahlin, K., Yao, K., Geng, S., Westman, G., Zhou, Q., ... & Rigdahl, M. (2017). Rheological properties of nanocellulose suspensions: effects of fibril/particle dimensions and surface characteristics. *Cellulose*, *24*(6), 2499-2510.

34. Jonoobi, M., Harun, J., Mathew, A. P., & Oksman, K. (2010). Mechanical properties of cellulose nanofiber (CNF) reinforced polylactic acid (PLA) prepared by twin screw extrusion. *Composites Science and Technology*, *70*(12), 1742-1747.

35. Trifol, J., Plackett, D., Szabo, P., Daugaard, A. E., & Giacinti Baschetti, M. (2020). Effect of crystallinity on water vapor sorption, diffusion, and permeation of PLA-based nanocomposites. *ACS omega*, *5*(25), 15362-15369.

36. Ghasemi, S., Behrooz, R., Ghasemi, I., Yassar, R. S., & Long, F. (2018). Development of nanocellulose-reinforced PLA nanocomposite by using maleated PLA (PLA-g-MA). *Journal of Thermoplastic Composite Materials*, *31*(8), 1090-1101.

37. Lo Re, G., Engström, J., Wu, Q., Malmström, E., Gedde, U. W., Olsson, R. T., & Berglund, L. (2018). Improved cellulose nanofibril dispersion in melt-processed polycaprolactone nanocomposites by a latex-mediated interphase and wet feeding as LDPE alternative. *ACS Applied Nano Materials*, *1*(6), 2669-2677.

38. Gabriel, V. A., Tousignant, M. N., Wilson, S. M., Faure, M. D., Cranston, E. D., Cunningham, M. F., ... & Dubé, M. A. (2022). Improving Latex-Based Pressure-Sensitive Adhesive Properties Using Carboxylated Cellulose Nanocrystals. *Macromolecular Reaction Engineering*, 2100051.

39. ASTM D882-18(2018), Standard Test Method for Tensile Properties of Thin Plastic Sheeting, ASTM International, West Conshohocken, PA, 2018, www.astm.org

40. ASTM D6287-17(2018), Standard Practice for Cutting Film and Sheeting Test Specimens, ASTM International, West Conshohocken, PA, 2018, www.astm.org

41. Ghasemi, S., Rahimzadeh-Bajgiran, P., Tajvidi, M., & Shaler, S. M. (2020). Birefringence-based orientation mapping of cellulose nanofibrils in thin films. *Cellulose*, *27*(2), 677-692.

42. Broadbent, S. R., & Hammersley, J. M. (1957, July). Percolation processes: I. Crystals and mazes. In *Mathematical proceedings of the Cambridge philosophical society* (Vol. 53, No. 3, pp. 629-641). Cambridge University Press.

43. Salaberria, A. M., H. Diaz, R., Andrés, M. A., Fernandes, S. C., & Labidi, J. (2017). The antifungal activity of functionalized chitin nanocrystals in poly (Lactid Acid) films. *Materials*, *10*(5), 546.

# APPENDICES

## APPENDIX A: SUPPLEMENTARY MATERIALS FOR CHAPTER 2

Table 4: Sieve Analysis of WF-CNF Furnishes

| Mixture | Fraction Diameter (μm) | Mass % |
|---|---|---|
| WF | >425 | 20.7 |
| | 250-425 | 56.1 |
| | <250 | 23.2 |
| WF-10%CNF | >425 | 33.4 |
| | 250-425 | 47.8 |
| | <250 | 18.8 |
| WF-30%CNF | >425 | 23.2 |
| | 250-425 | 52.6 |
| | <250 | 24.2 |
| WF-50%CNF | >425 | 36.5 |
| | 250-425 | 45 |
| | <250 | 18.5 |

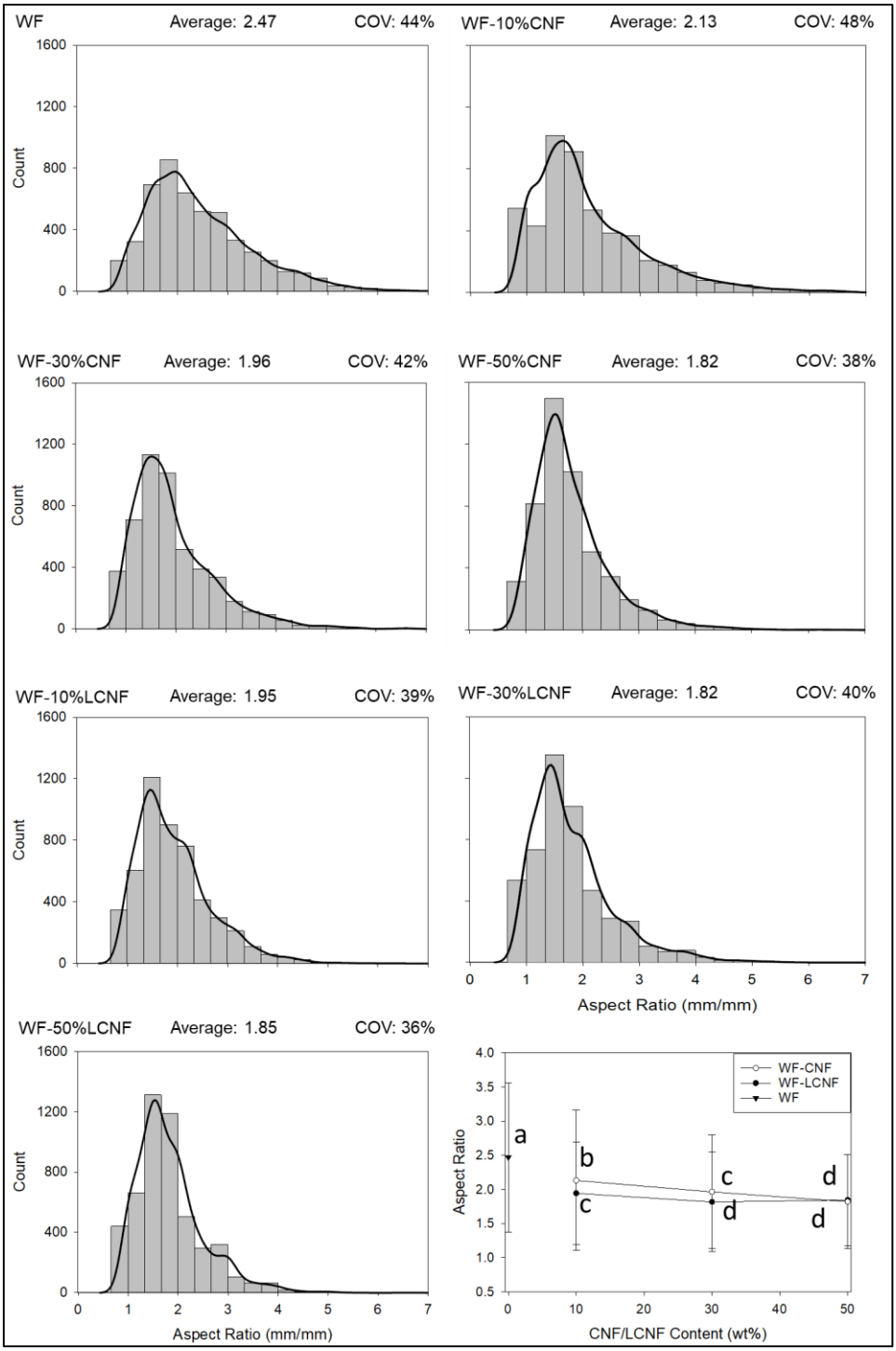


Figure 25: Histograms of aspect ratios (bin size = 0.33 mm/mm) from particle size analysis with kernel density overlays, (bandwidth = $1.616*10^{-1}$) and summary of average aspect ratios across all furnishes. Common letters on data points on the average comparison graph indicate statistically insignificant differences at 95% confidence level.

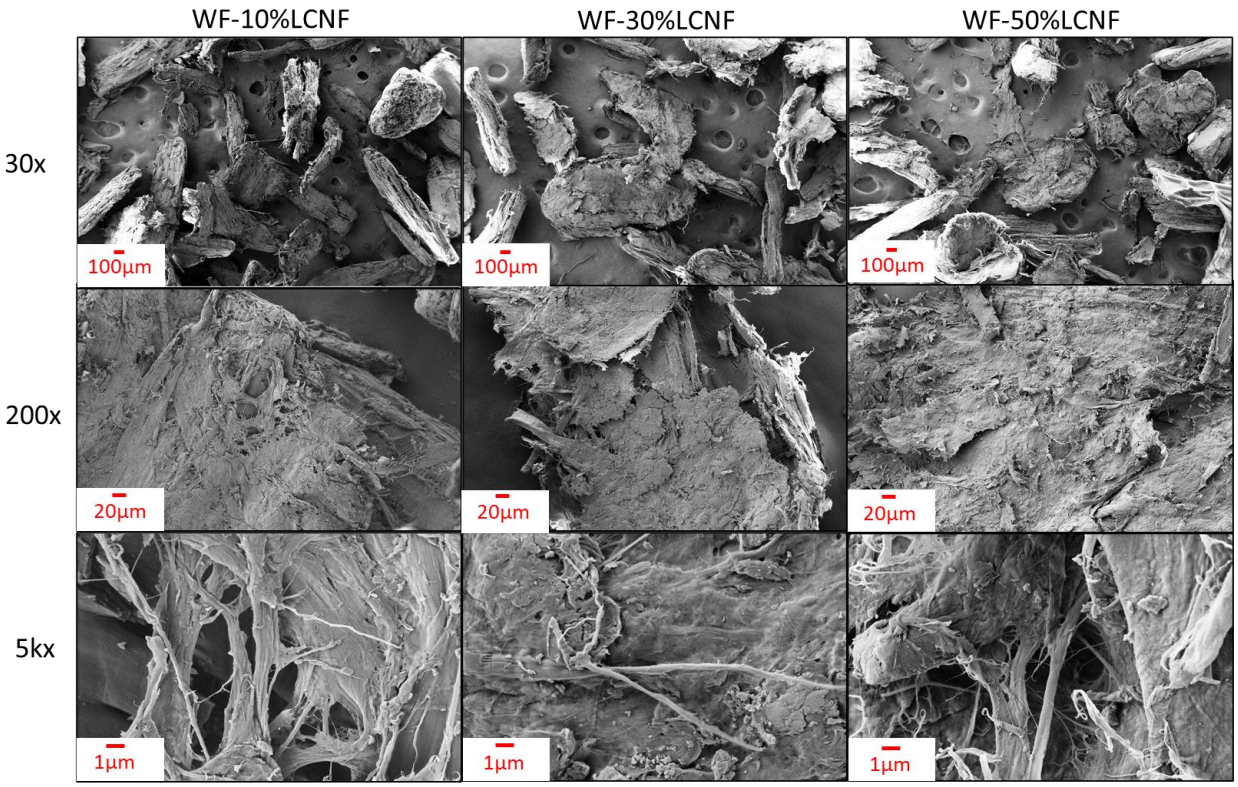


Figure 26: SEM Images of WF-LCNF furnishes. Top to bottom: 30x, 200x, 5kx magnification.

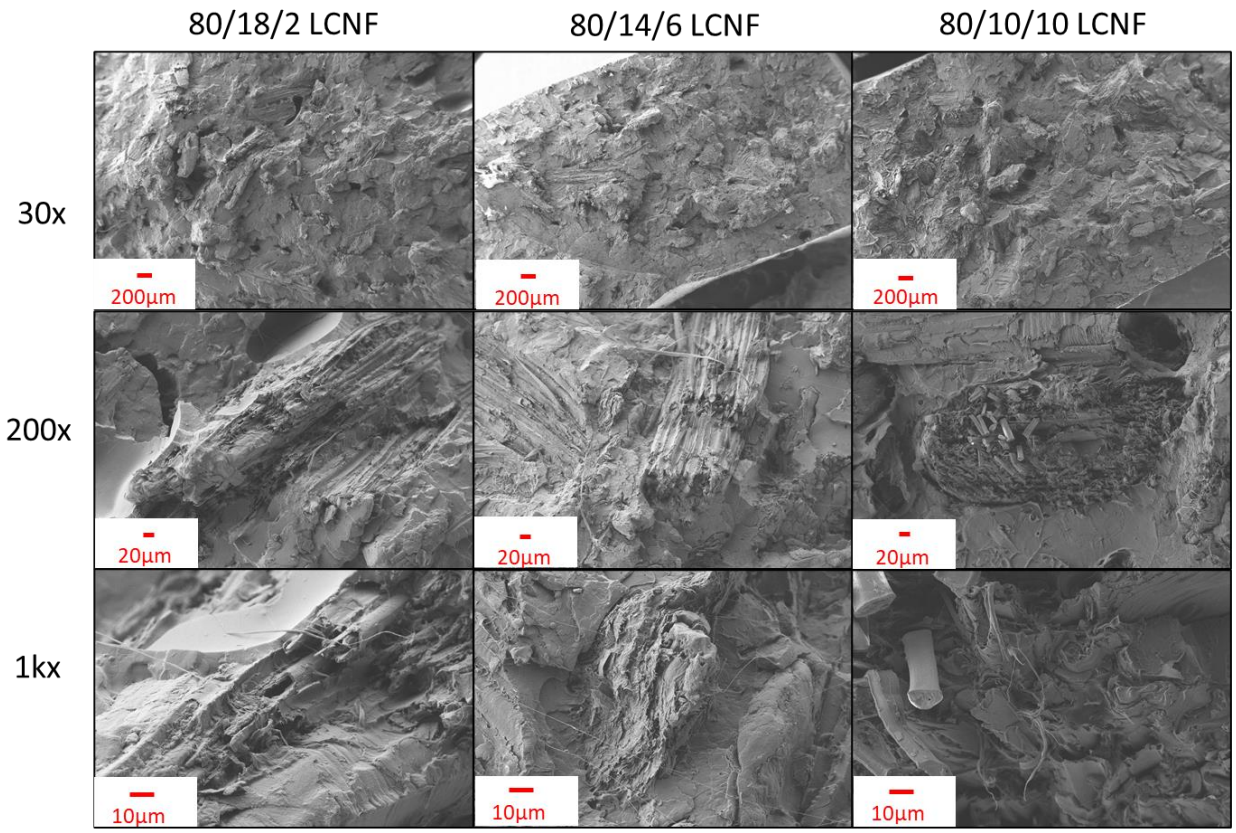


Figure 27: Tensile fracture surfaces from PLA/WF/LCNF Composites. Top to bottom: 30x, 200x, 1kx magnification.

# APPENDIX B: SUPPLEMENTARY MATERIALS FOR CHAPTER 3

Table 5: Summary of average shear-mixed PLA-CNF composite properties (with standard deviations) from tensile, and notched IZOD impact testing

| | | Tensile | | Flexural | | Impact |
|---|---|---|---|---|---|---|
| **Composite** | **CNF Type** | **Strength (MPa)** | **Modulus (GPa)** | **Strength (MPa)** | **Modulus (GPa)** | **Strength (J/m)** |
| PLA | N/A | 54.1 ± 1.2 | 3.52 ± 0.16 | N/A | N/A | N/A |
| PLA-0.5% | dCNF | 53.3 ± 2.8 | 3.51 ± 0.04 | N/A | N/A | N/A |
| PLA-1% | dCNF | 53.5 ± 1.8 | 3.66 ± 0.12 | N/A | N/A | N/A |
| PLA-2% | dCNF | 55.0 ± 1.1 | 3.67 ± 0.11 | N/A | N/A | N/A |
| PLA-10% | dCNF | 45.3 ± 1.5 | 3.48 ± 0.26 | 77.3 ± 4.2 | 3.16 ± 0.25 | 26.6 ± 2.1 |
| PLA-20% | dCNF | 41.0 ± 1.5 | 4.33 ± 0.64 | 71.8 ± 2.7 | 3.84 ± 0.28 | 28.8 ± 6.2 |
| PLA-30% | dCNF | 35.9 ± 2.0 | 4.55 ± 0.37 | 57.0 ± 5.8 | 4.26 ± 0.37 | 18.5 ± 3.8 |
| PLA-0.5% | SDCNF | 53.9 ± 1.6 | 3.42 ± 0.21 | N/A | N/A | N/A |
| PLA-1% | SDCNF | 53.7 ± 0.9 | 3.34 ± 0.11 | N/A | N/A | N/A |
| PLA-2% | SDCNF | 52.8 ± 0.5 | 3.43 ± 0.09 | N/A | N/A | N/A |

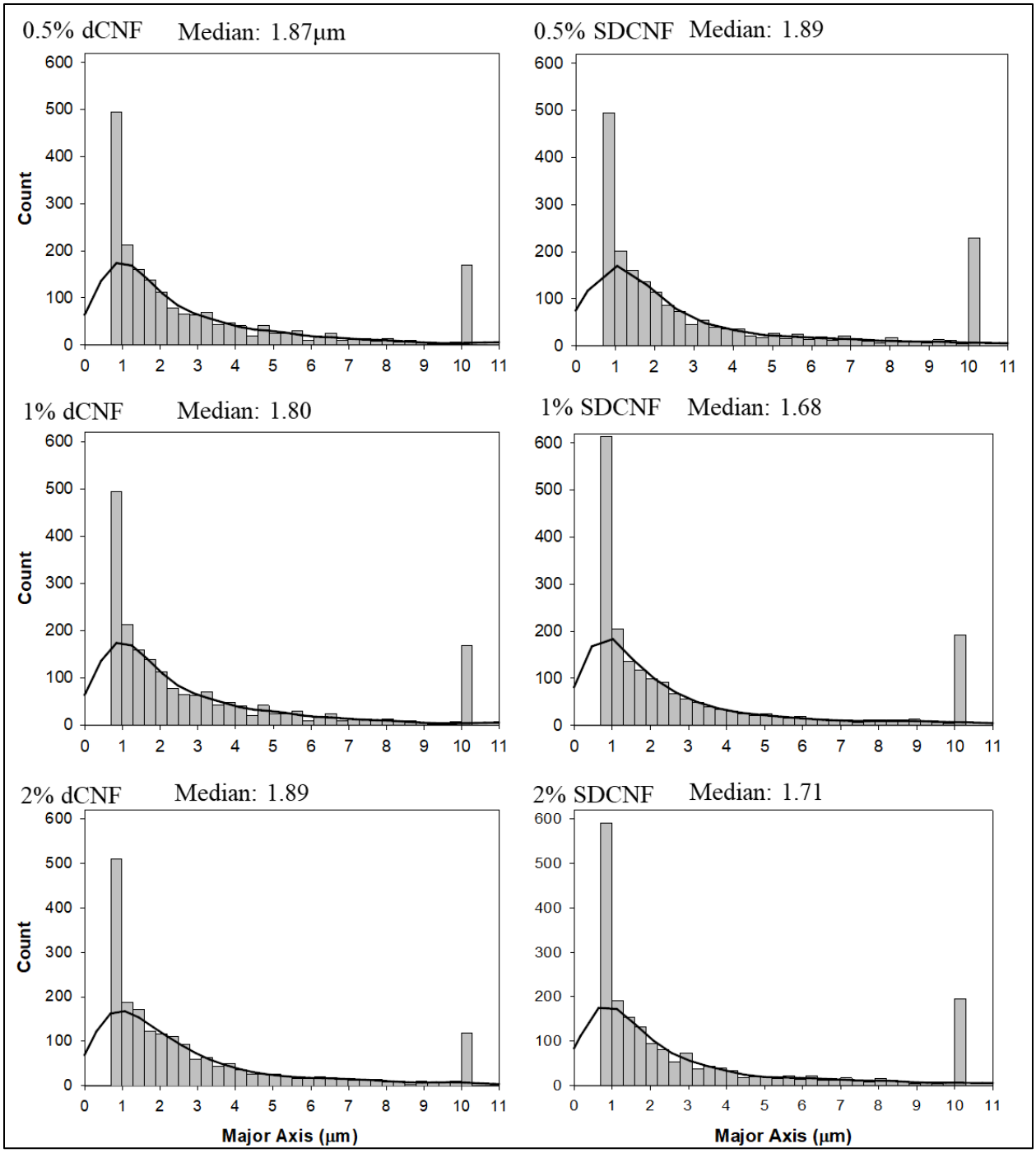


Figure 28: Histograms of major axis dimensions (bin size = 0.333 µm) from particle size analysis of PLM images with kernel density overlays, (bandwidth = $4.453*10^{-1}$).

## BIOGRAPHY OF THE AUTHOR

Alex was born in Detroit, Michigan, and, being an army dependent, spent his childhood living in Georgia, Hawaii, and Würzburg, Germany before his family finally settled in China, Maine. Alex received his undergraduate degree in Bioengineering at the University of Maine in 2015, and worked as an R&D and manufacturing scientist in Westbrook, Maine from 2016-2020. Here, he discovered his interest in materials science, and decided to combine that with his passion for environmental sustainability. It was this drive that led him to his M.S. in Forest Resources at UMaine, where he studied bio-based materials for manufacturing. His next steps are to continue his career in environmentally sustainable materials, with a focus on Life Cycle Assessments. Alex loves outdoor physical activities, including hiking, mountain biking, running, and skiing. He is also passionate about languages, philosophy, movies, music, and political activism. He is a candidate for the Master's of Science Degree in Forest Resources from the University of Maine August 2022.